The location of tropical precipitation in idealized atmospheric general circulation models forced with Andes topography and surface heat fluxes

Elizabeth Allison Maroon

A thesis submitted in partial fulfillment of
the requirements for the degree of

Master of Science

University of Washington

2013

Committee:

David Battisti

Dargan Frierson

Cecilia Bitz

Chris Bretherton

Program Authorized to Offer Degree:
Department of Atmospheric Sciences

©Copyright 2013
Elizabeth A. Maroon

University of Washington

Abstract

The location of tropical precipitation in idealized atmospheric general circulation models forced with Andes topography and surface heat fluxes

Elizabeth Allison Maroon

Chair of the Supervisory Committee:
Dr. David Battisti
Dr. Dargan Frierson

Department of Atmospheric Sciences

This aquaplanet modeling study examines how ocean heat transport (OHT) and topography influence the location of tropical precipitation. Two global atmospheric general circulation models from the GFDL hierarchy of models are used to test how the atmosphere responds to the same forcing. One model (GRaM) has simplified (gray) radiation and lacks cloud and water vapor feedbacks, while the other model (AM2) has more complex radiation, cloud processes, and feedbacks; both atmospheric models are coupled to a slab ocean. In both models, adding an Andes-like mountain range or adding realistic Andes topography regionally displaces rainfall from the equator into the northern hemisphere, even when wind-evaporation feedback is disabled. The relative importance of the Andes to the asymmetric hemispheric heating of the atmosphere by ocean transport is examined by including idealized and realistic zonally-averaged surface heat fluxes (also known as q-fluxes) to the slab ocean. A hemispherically asymmetric q-flux displaces the tropical rainfall toward the hemisphere receiving the greatest heating by the ocean. In the zonal mean, the displacement of rainfall from the equator is greater in simulations with a realistic q-flux than

with realistic Andes topography. Simulations with both a q-flux and topography show that the rainfall in the vicinity of the mountains is displaced slightly farther to the north in the region 50 (120) degrees to the west of the Andes in simulations using the GRaM (AM2) model than in simulations that only have a q-flux. In both models, the displacement of precipitation is always into the hemisphere receiving the greatest ocean heating, but the displacements in the simulations using the AM2 model are greater than those using GRaM. The output in GRaM shows that the atmospheric energy transport (AET) under-responds to a given OHT, while the cloud and radiative feedbacks active in AM2 result in an overcompensation of the AET. As a result, experiments using the AM2 model show a greater displacement of tropical precipitation from the equator.

TABLE OF CONTENTS

Page

List of Figures iii

List of Tables v

Chapter 1: Introduction and Background 1

Chapter 2: Models and Simulations 10

Chapter 3: Aquaplanet Control Climatologies 15

Chapter 4: Addition of a single southern hemisphere mountain range . . . 20
- 4.1 Changes in the hydrologic cycle 20
- 4.2 Changes in the energetic budget 30
  - 4.2.1 Changes in energy transport due to the addition of topography 30
  - 4.2.2 Attributing the energetic changes in the AM2 simulation with added topography 32
- 4.3 Changes to the circulation and the momentum budget 40

Chapter 5: Removal of wind-evaporation feedback 43
- 5.1 The response of removing wind-evaporation feedback in a flat aquaplanet 43
- 5.2 Removal of wind-evaporation feedback in simulations with a SH mountain range 47

Chapter 6: The climate response to the addition of both topography and surface heat fluxes 50
- 6.1 Zonal precipitation response in all simulations 50
- 6.2 An energetic analysis of the addition of q-fluxes in simulations with the same topography 53

6.3 An energetic analysis of the addition of topography in simulations with the same surface heating 60

Chapter 7: Summary and Conclusions 64

Bibliography 66

LIST OF FIGURES

Figure Number		Page
2.1	Topography and surface heat fluxes used in this study.	13
3.1	Streamfunction and zonal wind in AM2 and GRaM aquaplanet simulations	16
3.2	Total Gross Moist Stability and Total Gross Moist Stratification	17
3.3	Aquaplanet northward energy transport and zonal surface temperatures in AM2 and GRaM.	19
4.1	RTminusA precipitation change in AM2 and GRaM.	21
4.2	Lowest layer wind in AM2 RT simulation	22
4.3	Change in omega and meridional wind in IT AM2 simulation	23
4.4	RTminusA changes in precipitation, evaporation, moisture flux convergence, and moisture transport.	25
4.5	RTminusA changes of streamfunction and specific humidity in AM2 and GRaM	27
4.6	RTminusA changes in SST, evaporation, and low cloud in AM2 and GRaM.	29
4.7	Change in energy transport in simulations that include topography.	31
4.8	Difference in GRaM energy transport calculations using direct and indirect estimates.	33
4.9	RTminusA difference in energy transport calculations using direct and indirect estimates for GRaM simulations with varying numerics.	34
4.10	RTminusA changes in net total TOA radiation in AM2 and GRaM.	35
4.11	Schematic showing how changes in TOA absorbed radiation relates to NH-SH changes in radiation and cross-equatorial energy transport.	37
4.12	RTminusA NH-SH TOA net radiation change.	38
4.13	RTminusA change in surface zonal wind, upper troposphere zonal wind, and vorticity in AM2 and GRaM	42

5.1 Zonal mean changes in precipitation, evaporation, and wind in experiments with and without wind-evaporation feedback. 45
5.2 NoWESminusWES changes in specific humidity and streamfunction in AM2 and GRaM. 46
5.3 The impact of WES in setting the response to realistic topography. . 48
5.4 The difference between RT+NoWESminusNoWES and RTminusA of SST, evaporation and wind in AM2 and GRaM. 49
6.1 Zonally averaged precipitation in all AM2 and GRaM simulations. . . 51
6.2 ITCZ latitude versus cross-equatorial atmospheric energy transport and Global ITCZ location versus Pacific ITCZ location. 52
6.3 Compensation of atmospheric energy transport to the implied ocean energy transport. 54
6.4 Scaled TOA energetics for q-flux experiments. 56
6.5 Scaled NH-SH TOA energetics for q-flux experiments. 57
6.6 Change in energy transport in simulations that include topography. . 60
6.7 NH-SH TOA net radiation for topography simulations. 61

LIST OF TABLES

Table Number Page

2.1 Description of simulations discussed in this thesis. 14

4.1 Global mean surface temperature of GRaM and AM2 simulations. . . 41

ACKNOWLEDGMENTS

I wish to express my sincere appreciation to many individuals who have helped me in the course of this research and writing. Most importantly, I wish to thank my advisors David Battisti and Dargan Frierson for all of their guidance, advice, suggestions, ideas, and encouragement. I have learned so much from both of you and am excited that I will be learning even more from you both during the next few years. I would also like to thank Cecilia Bitz and Chris Bretherton for serving on my committee and for their spot-on advice regarding the research contained in this thesis. I appreciate all your suggestions and feedback very much.

There are a few other researchers who have helped me during the research on this Masters project. Brian Rose, now at SUNY Albany, has been a wonderful teacher. I am so grateful for all the time he spent with me going through model results and thinking about their implications. Neven Fučkar at the International Pacific Research Center has also been instrumental in teaching me about coupled ocean-atmosphere interactions and how to analyze the oceanic side of coupled results. I also appreciate all the great science conversations with Yen-Ting Hwang, Aaron Donahoe, Jack Scheff, Kyle Armour, Xiaojuan Liu, Matt Woelfle, and many, many others in the Department of Atmospheric Sciences.

I also wish to thank Marc Michelson, Harry Edmon, and David Warren for all of their computing help. In particular, Marc Michelson has been instrumental in helping me fix compilation issues and other problems with the models

on the clusters he monitors.

Thank you to the faculty of the Atmospheric Sciences Department for their friendliness, academic rigor, and collegiality. I also wish to thank the department staff (Kathryn Stout, Samantha Scherer, Debbie Wolf, Scott Sipes, Melissa Pritchard and others) for their tireless efforts to keep things running smoothly and to keep me on track. Thank you also to the graduate students and Grads10 for providing a fun, academic environment.

None of this would be possible without the generous funding of the National Defense Science and Engineering Graduate (NDSEG) fellowship which funded me for my first three years of graduate study. I also wish to acknowledge the IGERT Program on Ocean Change which funds me currently. The freedom to explore science without bounds has been a great experience.

And of course, a big thank you to my family and friends. Thank you Mom and Dad for always being there to encourage me and to Luke for your patience, caring, and love.

Chapter 1

INTRODUCTION AND BACKGROUND

The Intertropical Convergence Zone (ITCZ) is a region of low-level convergence and deep convection in the deep tropics over the oceans. Understanding the dynamics of tropical precipitation and its regional variations has implications for those living in the tropics. While our first-order knowledge of the location of tropical precipitation is sound, there is a key asymmetry that is not fully understood: more tropical precipitation falls in the northern hemisphere (NH) than in the southern hemisphere (SH). The purpose of this thesis is to probe some of the theories for this asymmetry and to test them in idealized general circulation models (GCMs).

The zonally averaged mean meridional circulation (MMC) in the tropics is the Hadley circulation, and has long been part of our conception of the tropical general circulation (Hadley, 1735). Precipitation occurs in the rising branch of the thermally direct Hadley Circulation. Rising air in the deep tropics hits the tropopause and travels toward both poles, carrying momentum and energy with it. Upon reaching the edge of the Hadley regime, now dry air subsides in the subtropics, radiatively cooling as it returns to the surface. In general, the deserts of the world are located in the subsiding branch of the Hadley circulation, though there are zonal asymmetries (e.g. in regions of monsoons, in paleoclimate evidence of a green Sahara). The surface branch of the Hadley cell flows equatorward, converging in the deep tropics and bringing moisture to the ITCZ, closing the cell.

Ignoring the influence of eddies at the edge of the Hadley cell, greater heating in the tropics is enough to drive the Hadley cell (Held and Hou, 1980). If the Hadley circulation conserved angular momentum in the absence of eddy effects, the subtropical

jet would be much stronger than observed. However, eddies are an important component of the tropical circulation and cannot be ignored. Eddies remove momentum from the jets, and control the strength of the Hadley cells. If we only consider eddy-momentum fluxes, it can be shown that eddies alone can drive the Hadley circulation (Vallis, 2005). Both eddy effects and angular momentum conservation are important for understanding the Hadley circulation in the tropics.

In an aquaplanet world with equinoctial insolation and without any other asymmetries or ocean circulation, the ITCZ would always be at the equator where TOA heating would be largest. The world, however, is not in a perpetual equinox state and the Hadley cells move with the seasons (Dima and Wallace, 2003). Ocean circulation and land-sea contrasts are important for the understanding the location of tropical precipitation. In an axisymmetric model, moving the peak surface temperatures even slightly off the equator has a large effect; the farther the peak temperature is from the equator, the stronger (weaker) the winter (summer) hemisphere Hadley cell becomes (Lindzen and Hou, 1988). The latitude of maximum temperature is equatorward of the zero streamline that separates the winter and summer Hadley cells. Incidentally, Lindzen and Hou (1988) remarked on the absence of a strong NH winter Hadley cell in the observations of the time, which would be associated with more tropical rain in the SH, something that was not observed. They thought that "given the lack of actual data south of the equator, it is perhaps premature to worry unduly about the discrepancy," but that "the distribution of surface temperature needs more careful and intensive measurement." This is precisely the ITCZ asymmetry that we are going to study here.

At first guess, one might expect that tropical precipitation would follow the maximum insolation, which is symmetric across the equator in the annual mean (Liou, 2002). This ignores all surface asymmeteries in continent configuration and radiative properties. The fact that we have more annual mean rain in the NH shows that these surface asymmetries must be important. In the annual mean, the ITCZ is in the

Atlantic and eastern Pacific ocean basins in the NH. Over the course of a year, either the ITCZ spends more time in the NH than in the SH or it is more intense during its time in the NH. Only for a brief time during March and April does the ITCZ in the Pacific approach the equator and dip southward, sometimes creating a double ITCZ (Adler et al., 2003; Mitchell and Wallace, 1992; Schumacher and Houze, 2003). The symmetric pattern of solar forcing alone is not sufficient to explain this asymmetry in tropical precipitation (Adler et al., 2003).

It is important to keep the zonal and regional pictures of tropical precipitation separate. Over land, tropical precipitation is nearly symmetric about the equator in the annual mean (Xie, 2005). Due to the land's smaller heat capacity, the highest surface temperatures (and highest surface heat flux) are closer in phase to the seasons than over the ocean. Tropical precipitation over land often follows the latitudes the greatest insolation through the seasons. In the western Pacific and over the maritime continent, where the thermocline is deep and there is the Pacific warm pool, precipitation is symmetric about the equator annually. In the Indian Ocean, annual mean precipitation is in the SH. Sea surface temperatures (SST) are high at the equator year-round in the Indian ocean. The presence of cold water upwelling is an important feature that distinguishes the dynamics of the Atlantic/Pacific from those of the Indian. To first order, the ITCZ is near the highest SST in the Atlantic and Pacific, which are north of the equator for the majority of the year, displaced by cold equatorial upwelling. For a discussion of how the SST maximum and the deepest ITCZ convection can be displaced by a few degrees of latitudes from each other in the tropics, see Tomas and Webster (1997). Zonal and annual-mean tropical precipitation is in the NH because it is in the NH of the Atlantic and Pacific ocean basins, and near the equator almost everywhere else (Mitchell and Wallace, 1992; Adler et al., 2003; Xie, 2005).

Besides equatorial upwelling in the eastern half of the Pacific and Atlantic ocean basin, there is cold water upwelling on the western edges of continents (ie, South

America), and large regions of stratocumulus in the subtropics (Klein and Hartmann, 1993). In the Pacific basin, temperatures are lower in the SH tropics and subtropics and an equivalently large region of cold temperatures does not exist north of the equator when examining the annual picture.

The equatorial cold tongue does not follow the semiannual cycle of insolation. During the equinoxes when there is highest insolation, one could expect the cold tongue to be decreasing in westward extent due to extra surface heating. During the solstices, the cold tongue might be expected to approach a maximum in extent due to less insolation. Observationally however, the cold tongue has a small extent (stays close to South America) during the April equinox, but extends farthest into the central Pacific during October (Mechoso et al., 1995). SST on the equator displays a strong annual cycle and a weak semiannual cycle, while the forcing from insolation has a strong semiannual cycle and no annual cycle. However, the Pacific warm pool does migrate semiannually with the seasons. In April it is in the SH; in October, the NH. This evidence indicates that ocean dynamics cannot be ignored in the determination of tropical SST structure.

In general, the cold tongue is symmetric across the equator. However, the ITCZ does not leap across it during the solstice seasons, staying completely in the NH during boreal summer and completely in the SH during austral summer. In addition, we only occasionally see a doubled ITCZ in March and April, but never in September and October. Giese and Carton (1994) tested the importance of the length of year on the seasonal cycle of the equatorial cold tongue and winds, as well as to tropical precipitation, in a GCM with slab ocean. Increasing the length of the year to 18 months allowed waters south of the equator to warm up enough during its summer such that the ITCZ moves completely to the SH. The cold tongue develops twice in this longer year, and the seasonal cycle of SST, winds and precipitation becomes semiannual on the equator as expected by a peak in insolation that crosses the equator twice yearly. Their model indicates that a 12-month year is not long enough to allow

the SH to warm up sufficiently to support more convection, but does not explain why this SH region is cooler than the same region in the NH. Observational and model studies suggested, but then discarded the involvement of the monsoon circulation in this NH preference for warmer waters and deep convection (Mitchell and Wallace, 1992; Giese and Carton, 1994). Eccentricity creates a difference in daily insolation between the NH and SH hemispheres in the Giese and Carton (1994) model; their results showed that eccentricity would favor a SH ITCZ.

Another study in 1994 proposed a feedback that sustains asymmetry across the equator, given an initial perturbation (Xie and Philander, 1994), similar to that discussed by Lindzen and Nigam (1987). Some initial perturbation causes slightly higher SST on one side of the equator than the other. Higher SST then induces lower sea level pressure (SLP) there, and sets up a pressure gradient across the equator. This drives flow across the equator. On both sides of the equator, these meridional winds are turned due to the Coriolis force. With warmer NH waters, anomalous southerlies are induced. These winds turn to the right in the NH, creating anomalous southwesterlies, and turn to the left in the SH, creating anomalous southeasterlies. In the SH, these anomalous winds act to increase the trade winds, which increases surface evaporation, and cools down the ocean in the SH. Conversely, in the NH, anomalous southwesterlies slow down the trade winds and decrease evaporation, increasing SST there. This serves to reinforce the temperature gradient across the equator, which feeds back on the circulation (Xie, 2005). The involvement of wind, evaporation and SST in this atmospheric feedback give it its name: the WES feedback. Coupled feedbacks can also become involved. Greater winds also drive more cold water upwelling which is another important feedback (Chang and Philander, 1994). Xie (1996) show that asymmetries originating in the eastern side of ocean basins are important and can an asymmetric signal westward. These feedbacks still do not address why the preference is for greater SST and rain in the NH tropics, only that a preference for one hemisphere over the other is possible, and that an initial double ITCZ state collapses

down to a single ITCZ in the simpler models of Chang and Philander (1994).

Philander et al. (1996) examine the importance of coastline configuration as the key equatorial symmetry-breaker in a GCM with no topography and a fixed SST surface. The hypothesis is that in the SH, greater upwelling (Ekman pumping) is caused by the southeasterly trades that are nearly parallel with the coast of South America in the eastern Pacific, and by southerly winds induced by land-sea contrasts along the African coast in the east Atlantic. In contrast, the northeasterly trades in the NH are perpendicular to the coast, which does not favor the upwelling of cold water. Colder water due to preferred coastal upwelling in the SH would be the crucial asymmetry for higher SSTs, favoring an ITCZ in the NH. However, in the GCM of Philander et al. (1996), air-sea interactions were not enough to create a strong precipitation asymmetry; the addition of stratus clouds in the model provided the necessary feedback. As seen in observations, stratus clouds exist in the eastern ocean basins of both the Pacific and Atlantic and work to decrease SST and increase stability (Klein and Hartmann, 1993). Clouds shade the ocean and cool it further, producing another positive feedback. WES feedback with these other feedbacks describe a feasible method by which an equatorially-symmetric climate can be pushed into an asymmetric one given a source of asymmetry in one hemisphere.

Takahashi and Battisti (2007) note a few inconsistencies with some aspects of the coastline theory: the most prominent being that the region of coastal upwelling along the coast of Peru is much smaller than the region of low SST. In their atmospheric model with an interactive mixed layer ocean, Takahashi and Battisti (2007) use the topography from the Rockies, Himalaya, and Andes to test the response of the climate system to topography changes. The Andes block westerly midlatitude flow and force subsidence of dry air toward the equator. Subsidence of dry air increases evaporation, which increases cooling of the ocean in the eastern SH Pacific ocean in a region larger than that described only by coastal upwelling. They also include combinations of other major mountain ranges along with the Andes, but find that since the Andes are

upstream of the other ranges, their influence on the subsidence in the tropics trumps that of the Rockies, leading to an ITCZ preference in the NH. The authors point to the Andes as a driving influence with respect to the NH ITCZ, and prefer to think of WES feedback starting from this initial orographic asymmetry. In response to the idea that topography leads to a NH ITCZ, Philander et al. (1996) noted the existence of ITCZ asymmetry in both the Atlantic and the eastern Pacific, and to the absence of an Andes-equivalent in Africa.

The mechanisms discussed thus far have been local in origin and response; a tropical forcing (topography, ocean upwelling, etc) leads to a tropical response. That the tropics can affect the climate of the extratropics is well-known, most notably by the response to ENSO in the extratropics (Liu and Alexander, 2007). However, a more recent line of research has shown that a remote forcing can affect the tropics, and the location of the ITCZ. Paleoclimate data provides evidence that temperature anomalies in one hemisphere are linked with the position of tropical precipitation (Koutavas and Lynch-Stieglitz, 2003; Peterson et al., 2000; Haug et al., 2001; deMenocal et al., 2000; Black et al., 1999; Thompson et al., 2000, for example). Model studies with radiative forcings or paleoclimate configurations, show precipitation moving to the warmer hemisphere (Chiang et al., 2003; Chiang and Bitz, 2005; Broccoli et al., 2006; Yoshimori and Broccoli, 2008, 2009, for example).

Kang et al. (2008) tested the hypothesis that the extratropics are important in an idealized atmosphere model with an aquaplanet slab ocean. The extratropics of one hemisphere were heated and the other cooled by an equal amount. In effect, these asymmetric q-fluxes simulate the ocean moving energy from one hemisphere to the other. In this study, the ITCZ and SST maximum are in the warmed hemisphere.

Kang et al. (2008) explain how changes in the extratropics effect the tropics in terms of energy transport. In the warmer hemisphere, less heat is diffused polewards, so less energy is transported poleward in this hemisphere. This energetic anomaly is eventually felt by the Hadley circulation. In the warmed hemisphere, the Hadley

circulation becomes more like a summer hemisphere circulation and is weaker than its counterpart in the winter hemisphere. Meanwhile, cooling in the opposite hemisphere has the opposite effect. Eventually this cold anomaly propagates to the Hadley region, and the circulation is also strengthened. More energy is transported poleward in the colder hemisphere to reduce the cross-equatorial heat difference created by the q-fluxes. The net effect of this process is an anomalous Hadley cell that transports heat in its upper branch from warmer to colder hemisphere. The surface branch, which moves in the opposite direction of the upper branch, converges moisture in the warmer hemisphere. The ITCZ is then in the warmer hemisphere.

The exact response of tropical precipitation to extratopical heating is model dependent. Both Kang et al. (2008) and Kang et al. (2009) note that the location of the ITCZ is sensitive to the convection scheme used in their idealized model. Kang et al. (2009) showed that the ITCZ moves farther from the equator in a more complex GCM that included water vapor and cloud feedbacks, as opposed to in the gray radiation atmosphere of Kang et al. (2008). The response of the ITCZ to extratropical heating is stronger with these feedbacks.

Studies by Frierson and Hwang (2012) and Hwang and Frierson (2013) support this energy constraint framework using CMIP3 and CMIP5 output (Climate Model Intercomparison Project). Frierson and Hwang (2012) show that changes in extratropical clouds and ice explain the majority of the tropical precipitation changes in CMIP3 2xCO2 slab simulations. Hwang and Frierson (2013) shows that cloud biases over the southern ocean are linked to the double ITCZ problem long experienced in GCMs (Zhang, 2001; Mechoso et al., 1995). Too few clouds in the southern ocean creates an anomalous warming compared to observations; in turn, this extra warming results in an extra SH ITCZ. CMIP3 and CMIP5 models that show have more southern ocean clouds are more likely to have a single NH ITCZ.

In the previous modeling studies of Kang et al. (2008) and Kang et al. (2009), the forcing in the extratropics is through a zonally-symmetric ocean heat flux (also known

as a q-flux) added to the surface energy equation in the mixed-layer ocean. These studies do not address whether a localized extratropical heating can create a zonal response in the tropics, or the importance of a dynamic ocean model. Fučkar et al. (2013) use an intermediate complexity coupled ocean-atmosphere model with a single rectangular ocean basin (Farneti and Vallis, 2009). They find that the hemisphere of greater heat release from the ocean to the atmosphere by deep water production is always the hemisphere of greater tropical precipitation. Deep water production occurs most in the sinking branch of the oceans meridional overturning circulation (MOC). Opening a circumpolar channel, much like the Drake Passage of the real world, anchors the sinking branch of the MOC to the NH. In turn, tropical precipitation is greater in the NH of this model. Zhang and Delworth (2005) show in the fully-coupled GFDL model that a decrease in the Atlantic MOC leads to a change in the Hadley circulation with a southward shift of convergence and precipitation.

The aim of this thesis is to understand how both local and remote forcing affect tropical precipitation in idealized models. A major focus of this study is the superposition of local forcing (through addition of a SH mountain range) with remote forcing (represented either by the ocean through either a q-flux in a mixed-layer model or by heat release in a fully dynamic model). Chapter 2 describes the hierarchy of models used in these experiments, briefly discusses any modifications made to these models, and outlines simulations. Chapter 3 gives a brief description of control climatologies in the two aquaplanet models used. Chapter 4 presents results from atmospheric GCMs with mixed-layer oceans when a SH mountain range is added. Chapter 5 adds q-fluxes alongside topography to gauge the relative impact of both types of forcings.

Theories that describe local forcing of the ITCZ often invoke the WES feedback. In Chapter 6, the wind dependence of evaporation is shut off in the atmospheric GCMs with slab oceans. Topography is again added, and the effect of a WES mechanism is judged by comparing runs with and without WES. Conclusions and future directions are presented in Chapter 7.

Chapter 2

MODELS AND SIMULATIONS

The right model should be chosen for the right problem. Simpler models may better illuminate the fundamental processes involved, but lack the complex details that better simulate a realistic climate. On the other hand, more complex models may hide the main processes under all the complexities and distort the big picture; they also to be computationally expensive. Using a hierarchy of models allows the comparison of results across levels of complexity and helps to identify the underlying processes at work (Held, 2005). In the results that follow, a variety of models from the GFDL model hierarchy have been used to see how adding layers of complexity changes the story, and if the results are robust.

The simpler model used in these studies is GRaM (Grey Radiation Model), an aquaplanet, grey radiation, moist atmosphere GCM (Frierson et al., 2006). It has a spectral dynamical core and is run in this study at T85 resolution with 25 vertical levels. All parameters are the same as those listed in Frierson et al. (2006) with two exceptions that evolved in the default model setup since that publication: the solar constant is set to 1368 W/m^2 and the critical Richardson number in the Monin-Obukhov boundary layer scheme is set to 2. A mixed layer ocean with a heat capacity of 1×10^7 $JK^{-1}m^{-2}$ closes the surface energy budget, which corresponds to a mixed layer depth of 2.4m. Such a shallow mixed layer depth decreases the integration time to equilibrium and has little effect on the mean state of the climate when compared to deeper mixed layer depths (Kang et al., 2009). Parametrized gravity wave drag is turned off. The model has moisture and precipitation, but no clouds or sea ice are represented. The insolation is set analytically to approximate the annual zonal

mean; there is no seasonal or daily cycle. To keep the globally averaged energy budget of the atmosphere near the observed budget, albedo is set to 0.31 everywhere. The longwave (LW) part of the calculation has one band with emissivity set by equatorial and polar optical depth parameters (grey radiation). Consequently, there are no cloud, ice, or water vapor radiative feedbacks in either the SW or LW bands. Large scale condensation is used for convection. These key simplifications allow the direct effect of moisture to be examined without its feedbacks included. The gray model has been modified to include q-fluxes.

The more complex model is an aquaplanet version of the AM2.1 atmosphere GCM with a finite volume dynamical core and a mixed-layer ocean (GFDL, 2004, 2006). The simulations of Kang et al. (2008) use the very similar AM2.0 setup. All fields that would produce an asymmetric radiative forcing (e.g., ozone) have been symmetrized across the equator. The radiative impact of aerosols is not included. Horizontal resolution is $2.5^\circ \times 2^\circ$ and there are 24 vertical hybrid pressure-sigma coordinate levels. The heat capacity of the mixed-layer ocean is 1×10^7 $\mathrm{JK^{-1}m^{-2}}$. Again, the shallow mixed layer depth decreases integration time and has little effect on the mean climate (Kang et al., 2008). AM2.1 (called simply AM2 from here forward) has more advanced physics than GRaM: complex radiation and cloud schemes are implemented, and unlike GRaM, cloud and water vapor feedbacks are present. A relaxed Arakawa-Schubert convection scheme is used for moist convection. The option for diurnally and seasonally varying insolation are present in the model, but for easier comparison to GRaM, annual mean insolation is used.

With each model, simulations were completed with idealized topography (IT) and realistic topography (RT) and with zonally symmetric idealized (IQ) and real-world (RQ) surface heat fluxes (Figure 2.1). In the IT simulation, a single mountain stretches from the equator to 52°S, is 10° wide, and peaks at 4000 m through the entire range. It is a simple representation of the Andes mountain range; much of these experiments draws inspiration from Takahashi and Battisti (2007). The RT

simulation uses real-world Andes topography interpolated with a spline fit to each models grid. The horizontal resolution of the two models is comparable, though not identical, which results in slightly different interpolations of the topography. The mountain ranges are actually "water mountains" as only the height of the surface, not the heat capacity, is changed.

Simulations were also completed with zonally-averaged surface heat fluxes (q-fluxes). The q-flux described in Kang et al. (2008) is used with two different amplitudes (IQ10 and IQ30) and is shown in Figure 2.1. The real-world zonally-averaged q-flux (RQ) is also used. It is derived from the CERES TOA energetic budget and the ERA-Interim atmospheric reanalysis (Wielicki et al., 1996; Dee et al., 2011), and is provided courtesy of Yen-Ting Hwang. To insure that the land does not introduce a spurious energy transport into this zonally-averaged q-flux, the values over land are set to zero. The implied ocean heat transport (OHT) of these q-fluxes indicates that heat is moved southward at all latitudes in IQ10 and IQ30, while in the RQ simulations the implied heat transport is generally poleward, but has a northward component at the equator (Figure 2.1, panel d). Additional experiments were conducted with both RT and all three q-fluxes.

To test the importance of the wind-evaporation feedback, the wind dependence of evaporation,

$$E = C_q|U|(q_{surf} - q_{atm})\mathbf{??} \tag{2.1}$$

is removed in both GRaM and the AM2 aquaplanet model. E is evaporation; C_q is the drag coefficient of moisture determined by Monin-Obukhov drag theory; $|U|$ is the absolute magnitude of the wind in the bottom atmospheric layer; q_{surf} is the surface specific humidity and q_{atm} is the specific humidity in the first layer of atmosphere. In the model $|U|$ is calculated using the surface wind magnitude and a gustiness parameter; in all simulations this gustiness parameter is zero. The gray radiation spectral model and aquaplanet AM2 models were re-written to read a netcdf of $|U|$

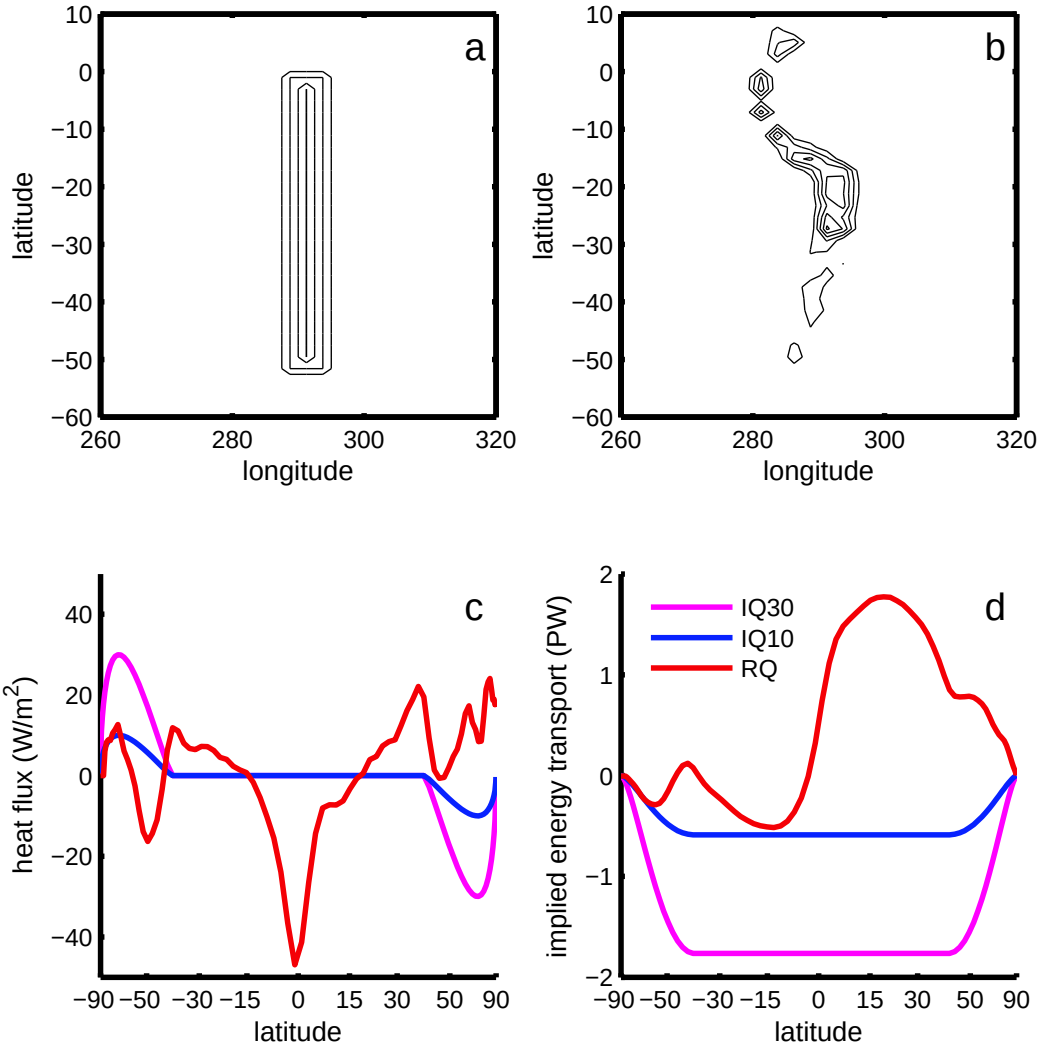

Figure 2.1: Topography and surface heat fluxes used in this study. a. "Idealized" SH mountain range topography with contours every 1000m. b. Realistic Andes topography with contours every 1000m. c. Zonal q-fluxes used in this study. Blue and magenta lines show the surface heat flux described in Kang et al. (2008) with peak amplitudes of 10 and 30 W m^{-2} at 65° latitude, respectively. The red line is the zonally-averaged surface heat flux as derived from CERES TOA energy and ERA reanalysis. d. The implied OHT for the surface heat fluxes in panel c. Note that latitude axis of panels c and d is area-weighted (sine of latitude).

Chapter	Models	Abbreviation	Description
3	GRaM/AM2	A	Aquaplanet only
4	GRaM/AM2	IT	Idealized Andes topography
	GRaM/AM2	RT	Realistic Andes topography
5	GRaM/AM2	noWES	Flat aquaplanet, no WES feedback
	GRaM/AM2	noWES + RT	Realistic Andes topography, no WES feedback
6	GRaM/AM2	IQ10	Kang et al. (2008) q-flux, amplitude of 10 W m^{-2}
	GRaM/AM2	IQ30	Kang et al. (2008) q-flux, amplitude of 30 W m^{-2}
	GRaM/AM2	RQ	Real-world zonally and annually averaged q-flux
	GRaM/AM2	RT+IQ10	Realistic Andes topography + Kang et al. (2008), amplitude of 10 W m^{-2}
	GRaM/AM2	RT+IQ30	Realistic Andes topography + Kang et al. (2008) q-flux, amplitude of 30 W m^{-2}
	GRaM/AM2	RT+RQ	Realistic Andes topography + real zonal q-flux

Table 2.1: Description of simulations discussed in this thesis.

at each lat/lon. Simulations in this study read in a $|U|$ from the flat aquaplanet simulation that is symmetrized about the equator. This prescribed $|U|$ is not used in the sensible heat or surface momentum flux equations.

Table 2 that lists all simulations that will be introduced in the following sections. All simulations were integrated with both GRaM and AM2. GRaM simulations were spun up for three years, while AM2 simulations were spun up for five years. Five additional years beyond the spin-up of each model are used for analysis. All results discussed in this paper are robustly defined using these averaging periods.

Chapter 3

AQUAPLANET CONTROL CLIMATOLOGIES

The mean climate of the control simulation (A) are remarkably similar GRaM and AM2, yet differ slightly which explain some the differences between the climate responses to various forcings. The jets in the GRaM control simulation are farther poleward than their counterparts in AM2 and the separation between the eddy-driven jet and the subtropical jet is seen more easily in GRaM (Figure 3.1). The atmospheric jet is faster in the AM2 model than in the GRaM model.

The Hadley cells in GRaM simulations are stronger than in AM2, as measured by the maximum in streamfunction at the cells' center (2.1×10^{11} kg s^{-1} in AM2 and 2.6×10^{11} kg s^{-1} in GRaM). However, the streamlines in AM2 are tighter in both its lower and upper branches, which results in greater mass flux concentrated at the top and bottom of the cells. Gross moist stability in the tropics is slightly larger in GRaM than in AM2 (Figure 3.2) because the total gross moist stratification in AM2 is larger in magnitude (both total gross moist stability and gross moist stratification are calculated as in Kang et al. (2009)). There is a small bit of asymmetry in gross moist stability and gross moist stratification because the separation of the NH and SH Hadley cells is slightly off the equator. Moisture is greatest in the lowest layers of the atmosphere, and dry static energy (DSE) is greatest high in the atmosphere because of the greater potential energy. Thus, differences in the vertical structure of the Hadley cells lead to differences in the amount of DSE and latent heat transport in the two models. In addition, the upper branch of the Hadley cells in GRaM is lower in the atmosphere than in AM2. Because there is little mass transport where DSE is greatest, the amount of poleward DSE transport in the tropics is less in GRaM than

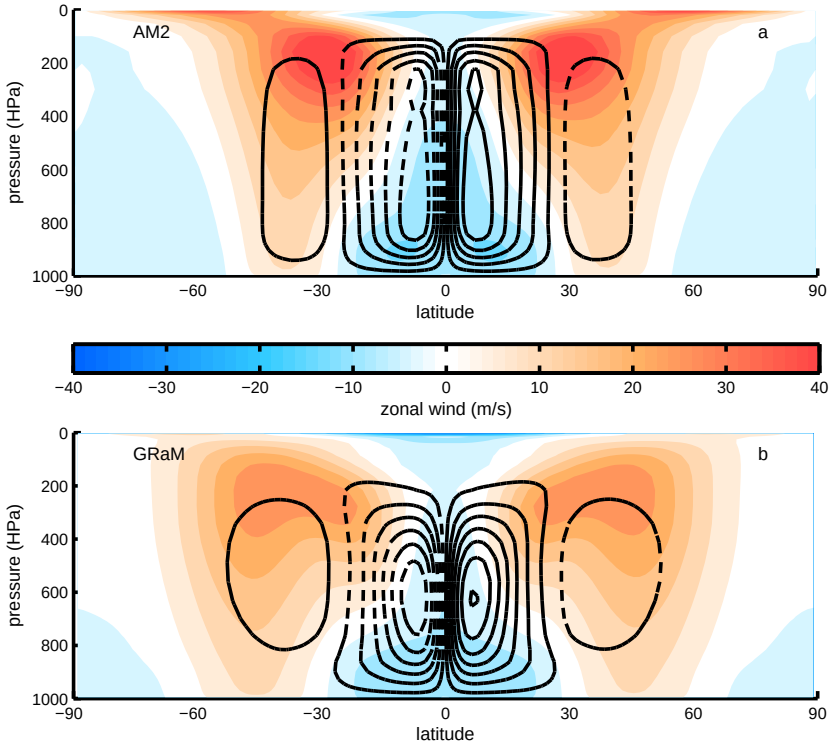

Figure 3.1: Aquaplanet simulation zonal wind (shading) and streamfunction (contours) in the AM2 model (panel a) and GRaM model (panel b). Solid contours indicate clockwise rotation while dashed contours show counterclockwise motion. The first solid/dashed contours are at +/- 2×10^{10} kg s^{-1} and subsequent contours are plotted every 4×10^{10} kg s^{-1}.

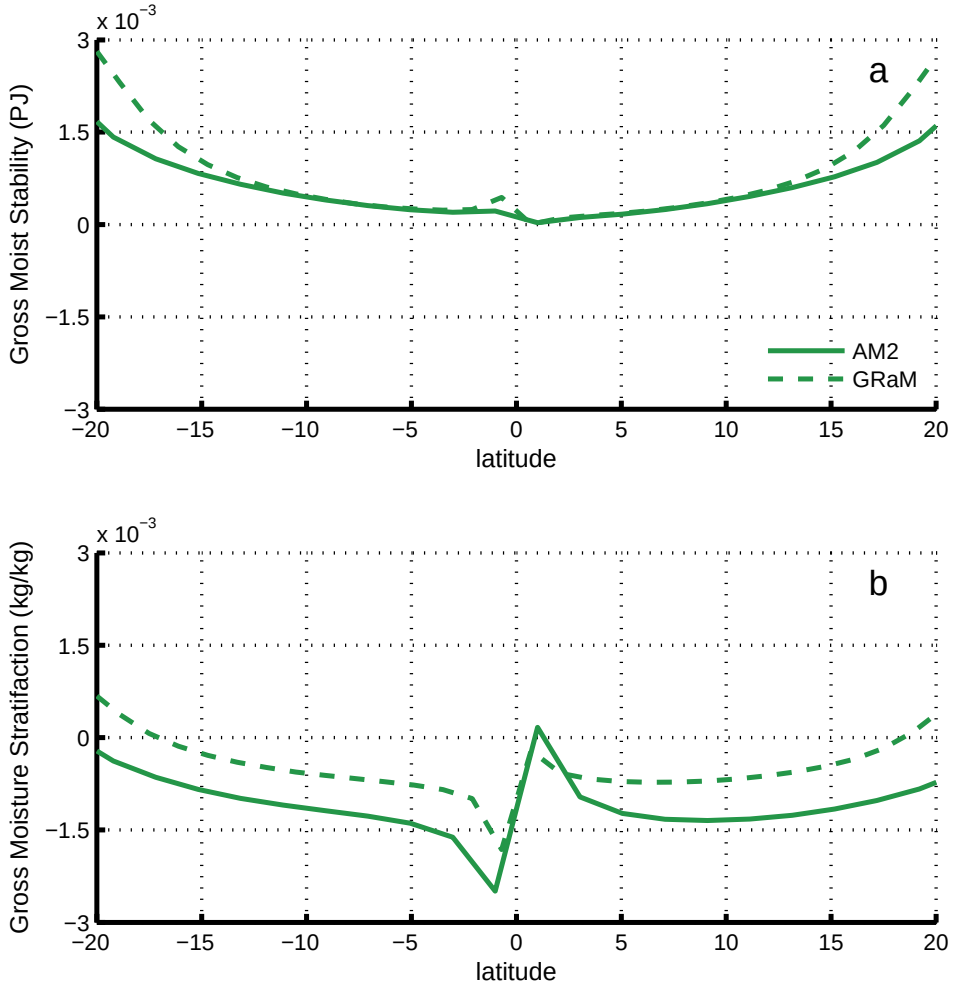

Figure 3.2: Total Gross Moist Stability (a) and Total Gross Moist Stratification (b) in the tropics of the AM2 (solid) and GRaM (dashed) aquaplanet simulations.

in AM2.

The total energy transport in GRaM is greater than that in AM2 because of the greater temperature gradient and DSE transport in the midlatitudes (Figure 3.3). In the tropics, the DSE and latent heat transports are larger in magnitude in the AM2 simulation than in the GRaM simulation. However, these energy transports compensate for each other better in the tropics of AM2. As a result, the total energy transport is less at all latitudes in the AM2 simulation than in the GRaM simulation.

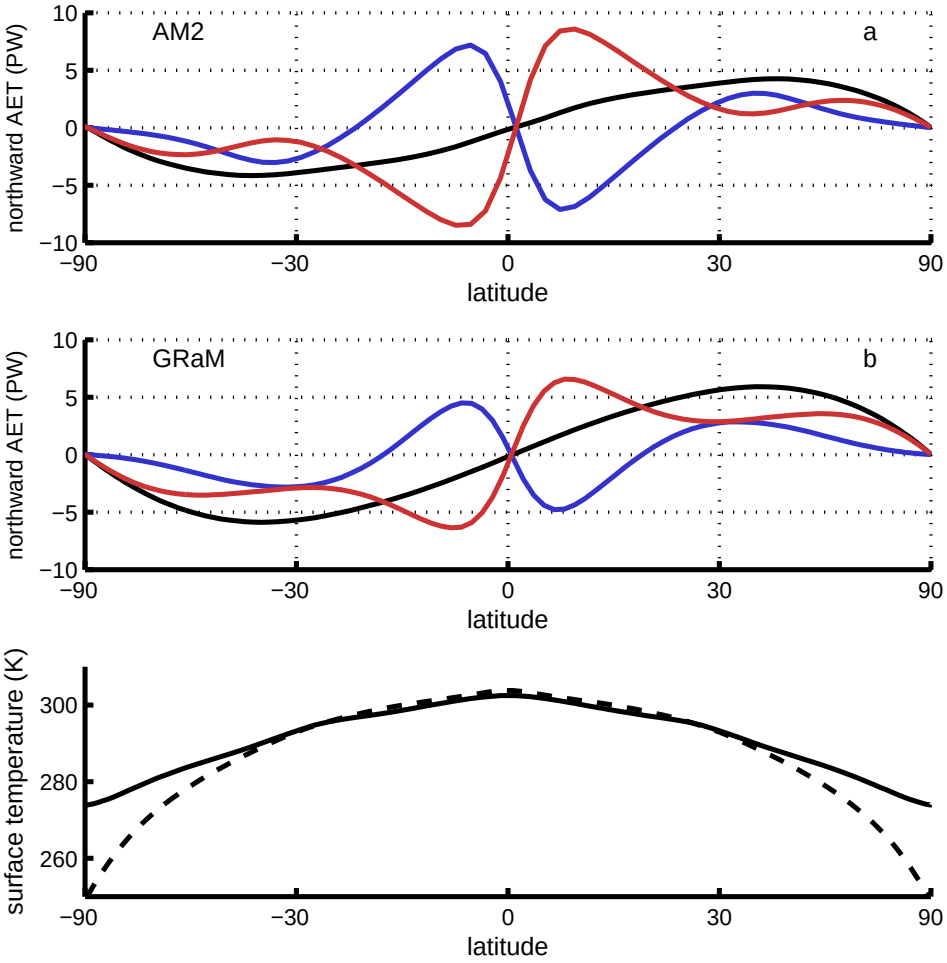

Figure 3.3: Aquaplanet northward energy transport and zonal surface temperatures in AM2 and GRaM. Panel a displays the northward total energy transport (black line), latent heat transport (blue line), and DSE transport (red line) in the aquaplanet only simulation in the AM2 model. Panel b displays the same energy transports for the aquaplanet GRaM simulation. Panel c shows the zonal surface temperature for this simulation. The solid line is for the AM2 model and the dashed line for the GRaM model.

Chapter 4

ADDITION OF A SINGLE SOUTHERN HEMISPHERE MOUNTAIN RANGE

The response of the centroid of precipitation in the IT and RT simulations are similar, which indicates that the exact structure of the mountain range does not play a large role. The response of tropical rain to IT is slightly greater because the spine of the IT range is 4000m for its entire extent, while the highest topography of the RT range is confined to the tropics and subtropics. Because of the similarity in the climate response with both mountain ranges, only results from RT simulations are shown here. The abbreviation RTminusA refers to the change in the climate caused by adding mountains compared to the flat aquaplanet simulation.

4.1 Changes in the hydrologic cycle

Placing a mountain range into both models creates subsidence to the west of the mountains as in Takahashi and Battisti (2007). When westerlies hit the mountain barrier in the subtropics and midlatitudes, they are deflected poleward and equatorward. Figures 4.2 and 4.3 show these changes in the AM2 IT simulation, and the same results are seen in GRaM simulations (not shown). Increased subsidence inhibits precipitation on the southern side of the equator, and the centroid of rainfall is displaced northward on the west side of the "Andes" in both AM2 and GRaM simulations (Figure 4.1 a and b).

The decrease in rain in the SH is greater than the increase of rain in the NH. There is a greater change of precipitation in the AM2 simulation than in GRaM; the precipitation anomalies have a greater zonal extent and magnitude in AM2. The

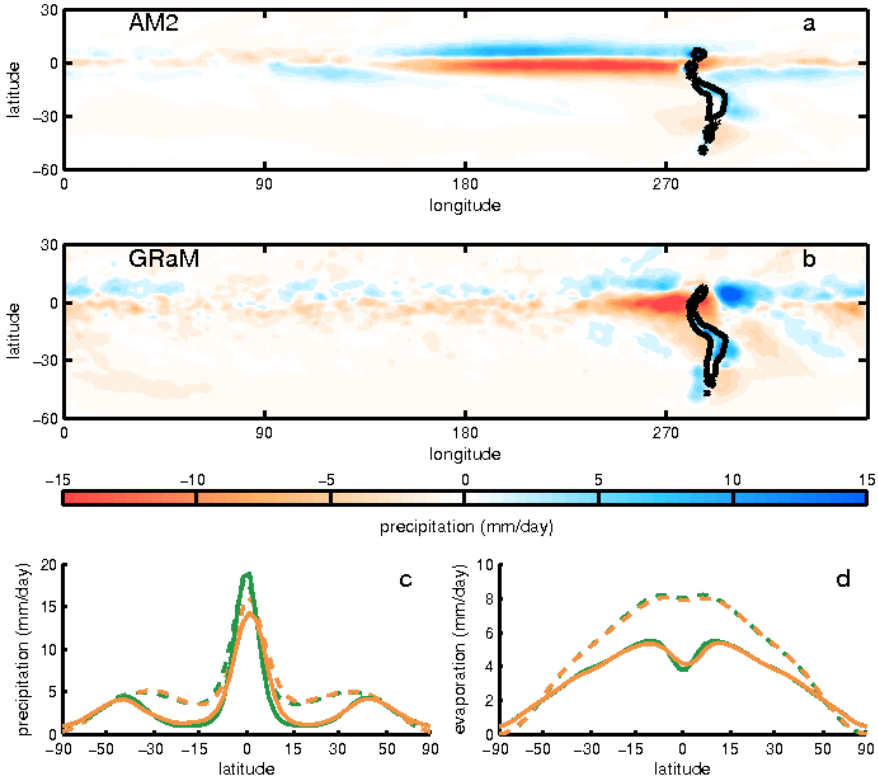

Figure 4.1: RTminusA precipitation in AM2 (panel a) and GRaM (panel b). Black contours indicates topography higher than 1000m. GRaM fields are Gaussian filtered (bandwidth of 5×10^{-4}). Zonally averaged AM2 (solid lines) and GRaM (dashed lines) precipitation (panel c) and evaporation (panel d) in the A (green lines) and RT (orange lines) simulations. Note that latitude axis of panels c and d is area-weighted (sine of latitude).

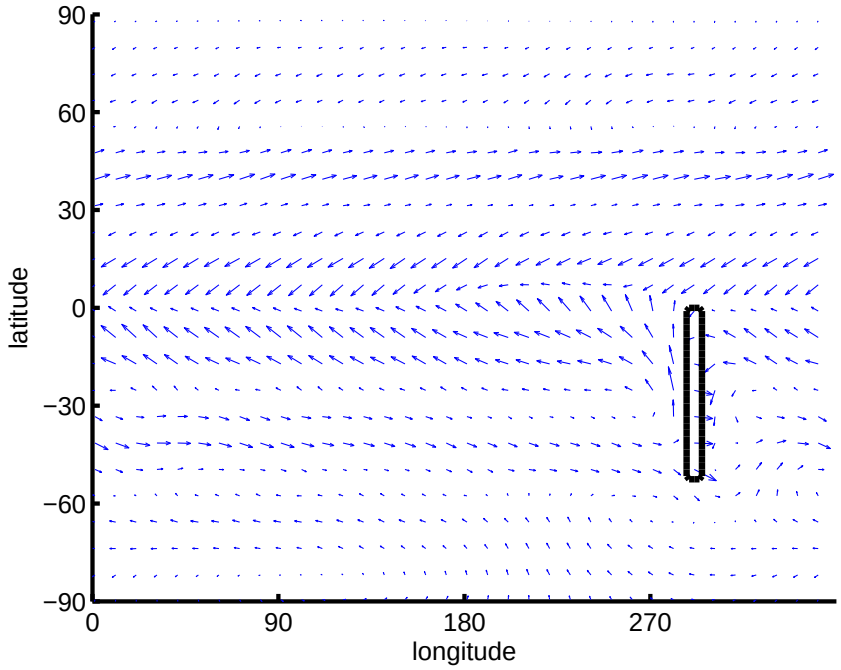

Figure 4.2: Lowest layer wind in the AM2 IT simulation.

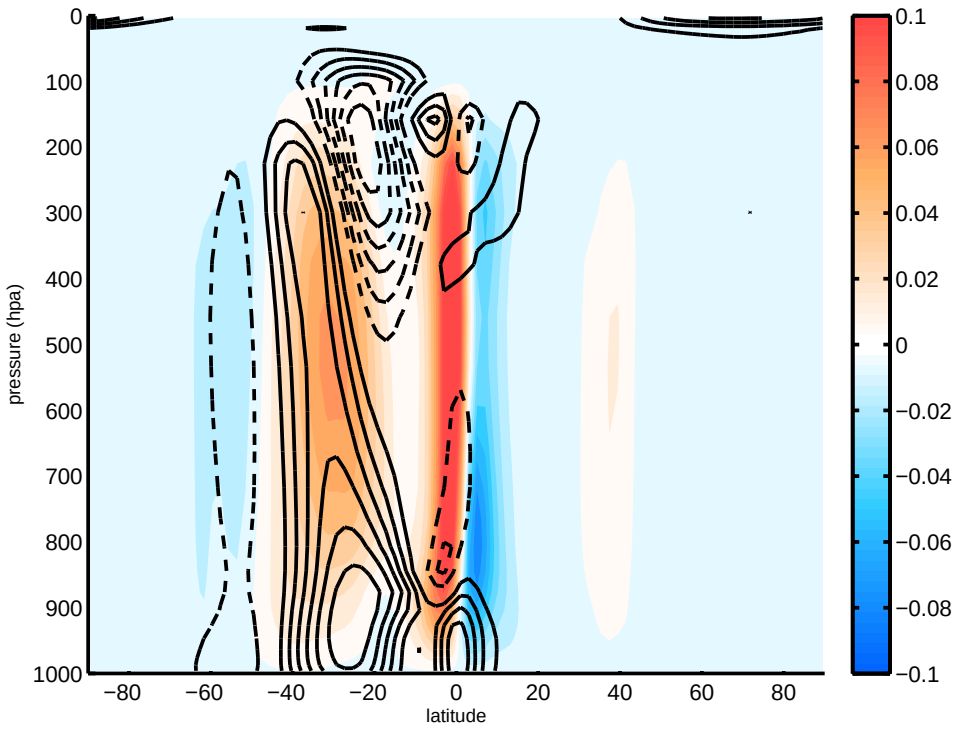

Figure 4.3: Change in omega (shading) and meridional wind (contours)in the IT simulation from the flat aquaplanet simulation in AM2 at 90W. Red indicates downward change in motion while blue indicates an upward change in motion. Solid contours show a northward change in meridional wind while dashed contours show a southward change.

influence of the Andes is seen 120° to the west in the AM2 RT simulation. The bulk of RTminusA northern displacement of tropical rainfall ends after about 50° of longitude in the GRaM simulation, although there is a small northward displacement of rain seen around the entire globe. In addition, the decrease of subtropical rainfall to the west of the Andes is larger in the AM2 simulation, even though the subtropics of this model are much drier (Figure 4.1c). As well as having drier subtropics, there is less precipitation in the tropics of the AM2 simulation than in the GRaM simulation. Both models' simulations see a decrease in the maximum tropical precipitation when adding topography. Evaporation (Figure 4.1d) does not change as much as precipitation when adding topography. AM2 simulations have a greater decrease of precipitation on the southward flank of the ITCZ, while the hemispheric changes in precipitation are more symmetric about the equator in GRaM.

The precipitation response to the east of the Andes is slightly different in the models. In GRaM, precipitation increases north of the equator before winds hit the topography. AM2 instead shows a weak increase of precipitation to the south of the equator. The large increase of precipitation east of the Andes in the RT GRaM simulation is not seen in the IT GRaM simulation. It is not a robust feature of the GRaM climate.

In steady state, the time and zonal mean moisture budget at the surface is described by

$$P - E = -\nabla \cdot [\overline{vq}]. \tag{4.1}$$

Using this budget, we decompose RTminusA precipitation (P) changes into changes in evaporation (E) and changes in vertically-integrated moisture flux convergence ($-\nabla \cdot [\overline{vq}]$). The majority of the increased precipitation are balanced by the convergence term (Figure 4.4). The change in AM2 evaporation has the opposite sign from the changes in precipitation, but is almost an order of magnitude smaller than the precipitation change; the GRaM RTminusA change in evaporation is negligible (Figure 4.4b). The moisture flux convergence when averaged both in time (marked

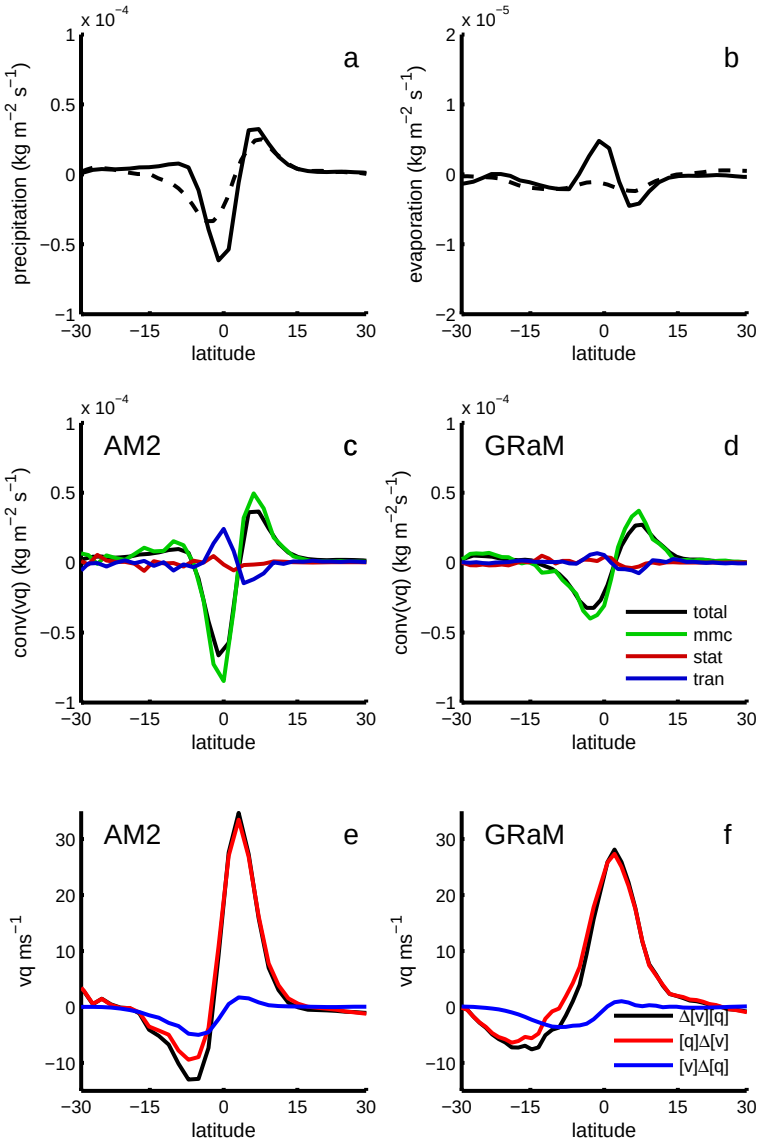

Figure 4.4: RTminusA changes in precipitation (panel a), evaporation (panel b), moisture flux convergence (panels c and d), and moisture transport (panels e and f). In panels a and b, the AM2 results are represented by solid lines and GRaM results by the dashed line. Panel c shows the decomposed moisture flux convergence for the AM2 RTminusA simulation. The total moisture flux convergence (black), the part from the MMC (green), the part from the stationary eddies (red) and the part from the transient circulations (blue) are all shown. The same decomposition for the GRaM RTminusA simulations is shown in panel d. Note that the y-axis in panel b is smaller than the y-axes in panels a, c, and d. Panels e and f show the RTminusA change in moisture transport (black line) for the AM2 (panel e) and GRaM (panel f) decomposed into $[\overline{q}]\Delta[\overline{v}]$ (red line) and $[\overline{v}]\Delta[\overline{q}]$ (blue line).

by overbars) and zonally (denoted by brackets) can then be further decomposed (as in Peixoto and Oort (1992) for example) into

$$-\nabla \cdot [\overline{vq})] = -\nabla \cdot [\overline{v}][\overline{q}] - \nabla \cdot [\overline{v^* q^*}] - \nabla \cdot [\overline{v' q'}]. \tag{4.2}$$

Terms with asterisks are the anomalies from the zonal mean, and terms with primes are the departure from the time mean. The first term on the right hand side of the equation represents the portion of the moisture flux convergence that is attributed to the mean meridional circulation (MMC). The second term is the part from the stationary eddies and the third term is the part from all transient circulations. Decomposing the zonally-averaged, time-averaged moisture flux convergence into these terms shows that the majority of the change in moisture flux convergence is due to changes in the MMC term (Figure 4.4c and d). Although one might first think that adding mountains would result in a change that is largest in the stationary eddy term, this is not the case. While the zonal anomalies of specific humidity and meridional wind do

In both models, adding a SH mountain range results in a change to the tropical MMC (the Hadley cells), which occurs mostly in the region to the west of the mountains. Figure 4.5 shows the change in zonal and time mean streamfunction and specific humidity. This figure helps to diagnose if the RTminusA changes in $-\nabla \cdot [\overline{v}][\overline{q}]$ are related to changes in meridional wind, changes in moisture, or both. The streamlines indicate that an anomalous cross-equatorial Hadley cell transports more moisture into the NH. Moisture has decreased in the SH tropics and subtropics and increased in the mid-troposphere of the NH tropics coincident with the anomalous Hadley cells ascending branch (Figure 4.5).

It can be shown that:

$$\Delta([\overline{v}][\overline{q}]) = [\overline{q}]\Delta[\overline{v}] + [\overline{v}]\Delta[\overline{q}], \tag{4.3}$$

where for a given quantity $[\overline{X}]$, $[\overline{X}] = ([\overline{X_{RT}}] + [\overline{X_A}])/2$ and $\Delta[\overline{X}] = [\overline{X_{RT}}] -$

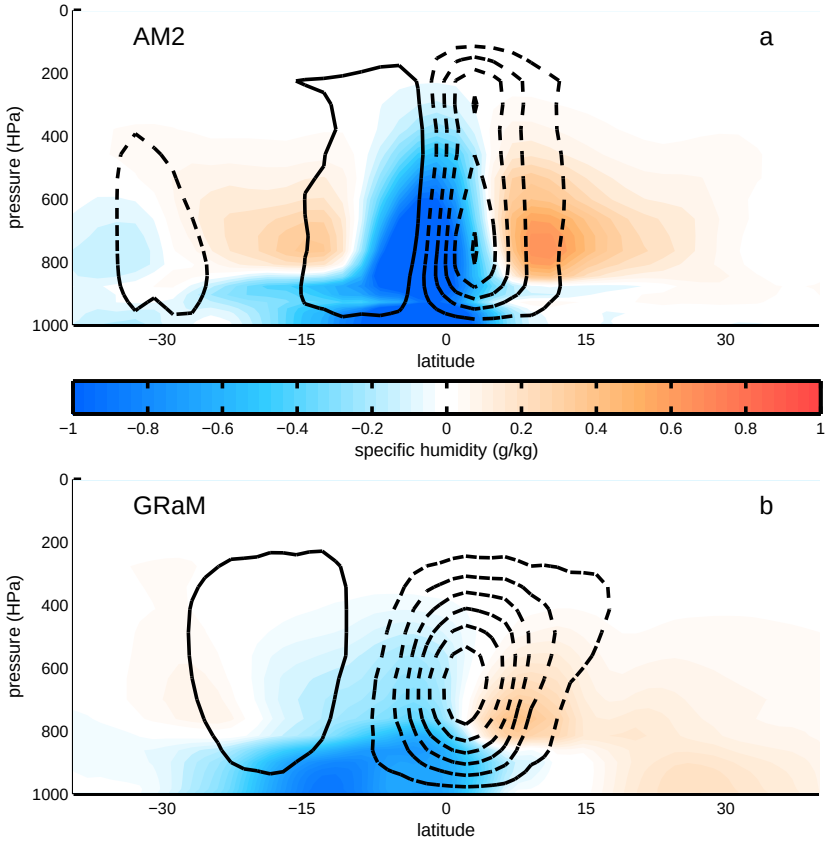

Figure 4.5: RTminusA changes of streamfunction (contours) and specific humidity (shading) from adding mountains in AM2 (panel a) and GRaM (panel b). Streamlines are displayed every 2×10^{10} kg s^{-1}, starting at the 1×10^{10} kg s^{-1} contour. Solid contours indicate clockwise motion while dashed contours indicated counterclockwise motion. For comparison, the maximum Hadley cell streamfunction in the mean climate in either model is near 2.5×10^{11} kg s^{-1}.

$[\overline{X_A}]$. Figure 4.2e and f show that both terms on the right hand side of Equation 4.3 contribute positively to RTminusA changes in moisture transport, but the first term is larger. Changes in the circulation term ($[\overline{q}]\Delta[\overline{v}]$) account for more of the change in moisture transport than changes in the specific humidity. Taking the meridional derivative of $[\overline{q}]\Delta[\overline{v}]$ gives us moisture flux convergence in terms of two quantities: $\frac{\partial[\overline{q}]}{\partial y}\Delta[\overline{v}]$ and $[\overline{q}]\frac{\partial\Delta[\overline{v}]}{\partial y}$. The wind convergence change term $[\overline{q}]\frac{\partial\Delta[\overline{v}]}{\partial y}$ shows the most change (not shown).

The same general meridional pattern of precipitation change exists in both models, and the dominant terms ($[\overline{q}]\Delta[\overline{v}]$) that balance the changes in precipitation are similar in both models. Hence, it is likely that whatever mechanism pushes precipitation northward does not need to rely on cloud feedbacks, as GRaM has no clouds. In the GRaM simulations, the area of increased SH evaporation due to the presence of the mountains is very narrow along the equator (Figure 4.6). The anomalous winds across the equator are very small in GRaM. These differences in the amplitude and spatial structure of the response in AM2 and GRaM to mountains are due to cloud feedbacks, which are important in AM2, but not allowed in GRaM.

In AM2 simulations, increasing SH subtropical subsidence increases the large stratus decks there, cooling the surface and decreasing evaporation (Figure 4.6a). There are also enhanced cross-equatorial winds in AM2, and the pattern of anomalous evaporation near the equator would potentially indicate a WES feedback. However, the strongest decrease in SST coexists with the greatest increase in the stratus cloud deck. Stratus clouds could further cool waters and reinforce subsidence, favoring even more stratus clouds, while decreasing evaporation. This subsidence would inhibit convection in the SH, thereby preferring a NH ITCZ, without needing to invoke any WES feedbacks. In a later section, wind-evaporation feedback will be turned off through the evaporation parameterization to see if the models can support NH tropical rainfall without WES.

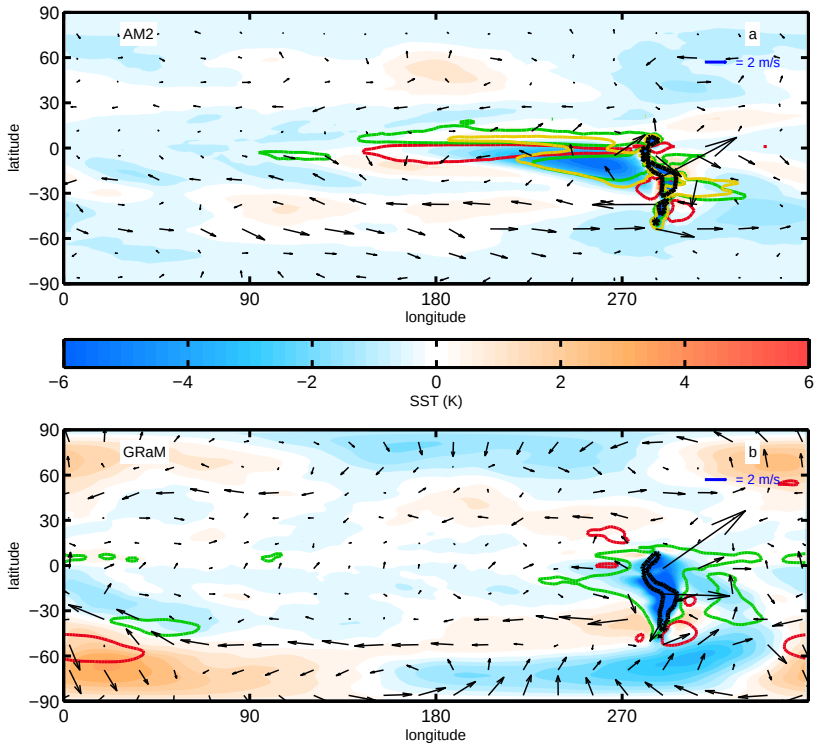

Figure 4.6: The RTminusA changes in SST (shading), evaporation (positive change for red and negative change for green contours), and low cloud (yellow contour) in AM2 (panel a) and GRaM (panel b). Green (red) contours indicate a 10 W m^{-2} decrease (increase) in evaporation in AM2 and a 5 W m^{-2} decrease (increase) of evaporation in GRaM. Vectors represent the change in the winds of thebottom sigma layer. The yellow contour in panel a indicates where low clouds in AM2 increased by more than 10%. Black contours indicates topography higher than 1000m. GRaM fields are Gaussian filtered (bandwidth of 5×10^{-4} m^{-2}).

4.2 Changes in the energetic budget

4.2.1 Changes in energy transport due to the addition of topography

The addition of topography to each model changes the flow of energy between the hemispheres. Figure 4.7 shows the RTminusA difference in zonally-averaged atmospheric energy transport (AET) of each topography simulation. In AM2, adding topography results in an anomalous transport of heat from the NH to SH (Figure 4.7). This southward transport of heat is accomplished by the upper branch of an anomalous Hadley cell (Figure 4.5).

In GRaM, the change in atmospheric energy transport becomes complicated: depending on how you calculate energy transport, the changes in energy transport change. Using a direct method that takes the vertical integral of moist static energy transport (vMSE) gives a different estimate than using the more indirect method that uses a horizontal integral of the TOA radiation imbalance. These estimates differ by as much as 0.3 PW in some locations for every GRaM simulation presented in this thesis (Figure 4.8). The differences in the energy transport estimates are greatest in simulations that include topography. As a result, the change in the RTminusA estimate of energy transport at the equator has different signs with the two estimates. Figure 4.7 shows the RTminusA difference using the direct calculation. There is noise because GRaM has a spectral core. The structure compares well with that from AM2, however, using the TOA budget to calculate the same quantity gives an anomalous northward energy transport from adding topography (Figure 4.9). Varying the timestep and the vertical resolution does not change the difference between these two estimates. Using a Betts-Miller convection scheme instead of the large scale condensation does not change the estimates, and using higher horizontal resolution is also not effective at bringing the two estimates closer (not shown).

Both estimates are as exact as possible, and neither can be considered more correct over the other. Examining the TOA budget shows that the reason for the anomalous

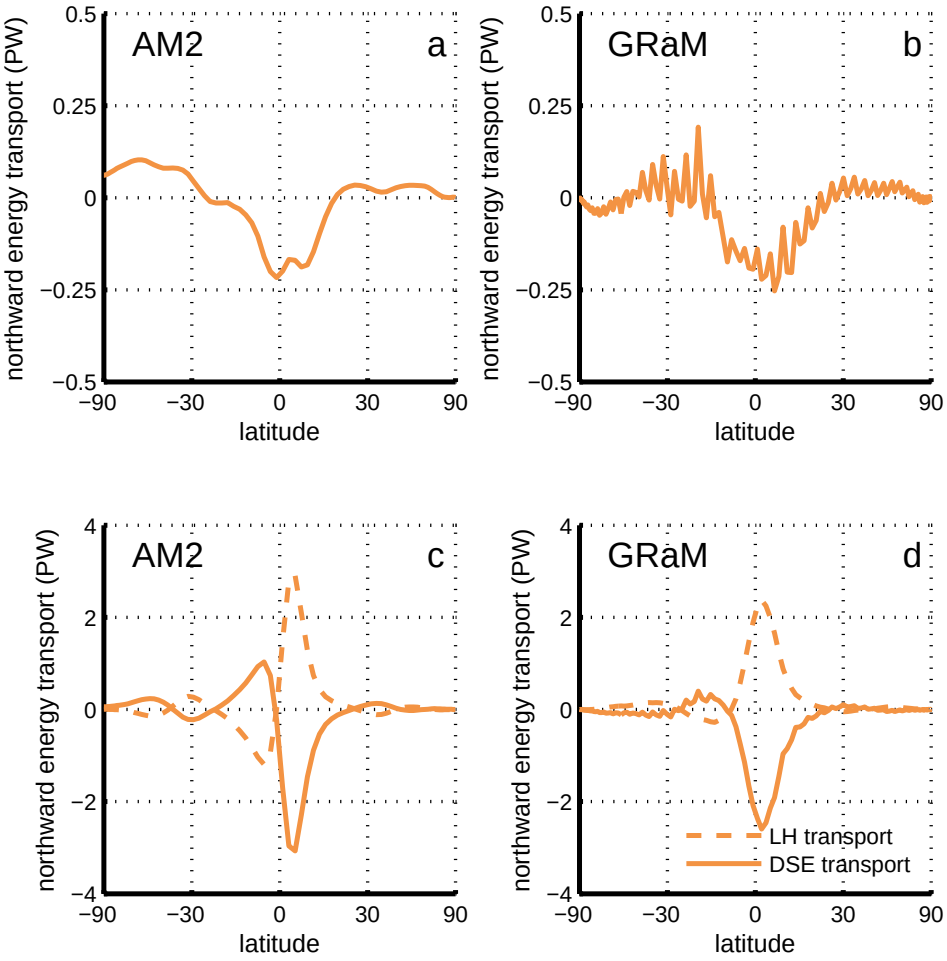

Figure 4.7: Change in energy transport in simulations that include topography. Panel a and b show the change in total energy transport in AM2 and GRaM simulations that include topography from their equivalent flat simulations. Panels c and d show the change in DSE (solid) and latent heat transport (dashed) in the RTminusA AM2 and GRaM simulations.

northward energy transport (which would suggest a thermally indirect anomalous Hadley cell) is due to less OLR in the SH than in the NH (Figure 4.10). These results suggest that there is an additional energy loss in the model due to numerics near the mountains. In GRaM, there is normally some energy loss. During each step of integration, the energy loss is determined and replaced by adding a constant temperature to every grid point. In our simulations that do not have topography this temperature correction is on the order of 2.8×10^{-4}K, which corresponds to an energy loss of approximately 2 W m^{-2}. In the RT simulation, the temperature correction is 6.8×10^{-4}K, which is about a 7 W m^{-2} energy loss. This greater energy correction is more evidence that topography causes an extra northward numerical diffusion of energy. It is possible that this numerical energy transport could be a forcing for the southward transport of moist static energy (as seen in the direct calculation). It suggest that these numerical issues may be the driver behind why there is greater tropical precipitation in the northern hemisphere of the RT GRaM simulation.

4.2.2 Attributing the energetic changes in the AM2 simulation with added topography

Another way to examine the cross-equatorial energy transport is to examine the top-of-atmosphere (TOA) radiative imbalance between the two hemispheres.

$$\Delta OET^{\phi=eq} + \Delta AET^{\phi=eq} \equiv \Delta TET^{\phi=eq} \tag{4.4}$$

$$\begin{aligned} \Delta TET^{\phi=eq} &= \int_{-\pi/2}^{0} 2\phi a^2 \cos(\phi)(\Delta SW - \Delta OLR)d\phi \\ &= -\int_{0}^{\pi/2} 2\pi a^2 \cos(\phi)(\Delta SW - \Delta OLR)d\phi, \end{aligned} \tag{4.5}$$

where ϕ is latitude, a is the radius of the Earth, $\Delta OET^{\phi=eq}$ is the change in ocean energy transport at the equator, $\Delta TET^{\phi=eq}$ is the total meridional energy transport at the equator, ΔSW is the change of net shortwave radiation (with positive defined as into the atmosphere) and ΔOLR is the change in outgoing longwave radiation (with positive defined as leaving the atmosphere). In the integral, the equator is 0 and the

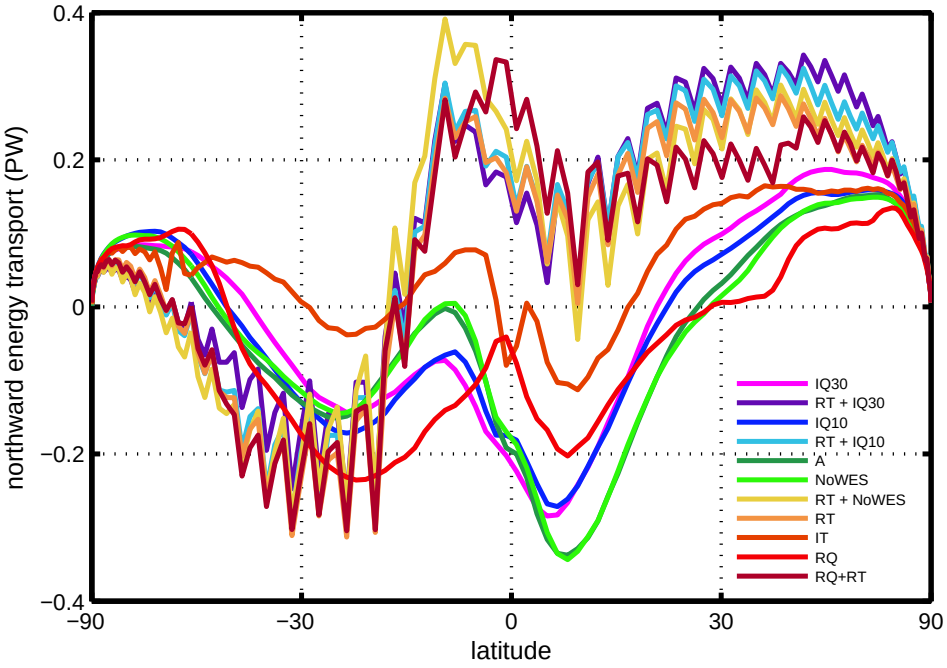

Figure 4.8: The difference in the energy transport calculations for GRaM simulations using direct and indirect methods.

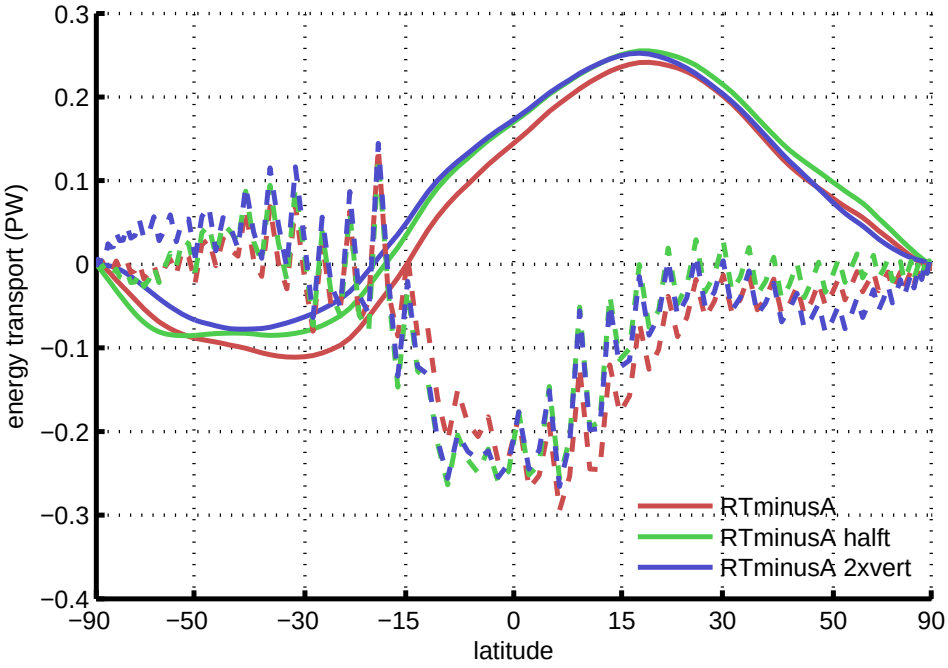

Figure 4.9: The RTminusA difference in the energy transport calculations for GRaM simulations using direct (dashed lines) and indirect (solid lines) methods. The included RTminusA simulations in this figure have the default time step and vertical resolution (red), a halved time step (green), and a halved time step with doubled vertical resolution (purple).

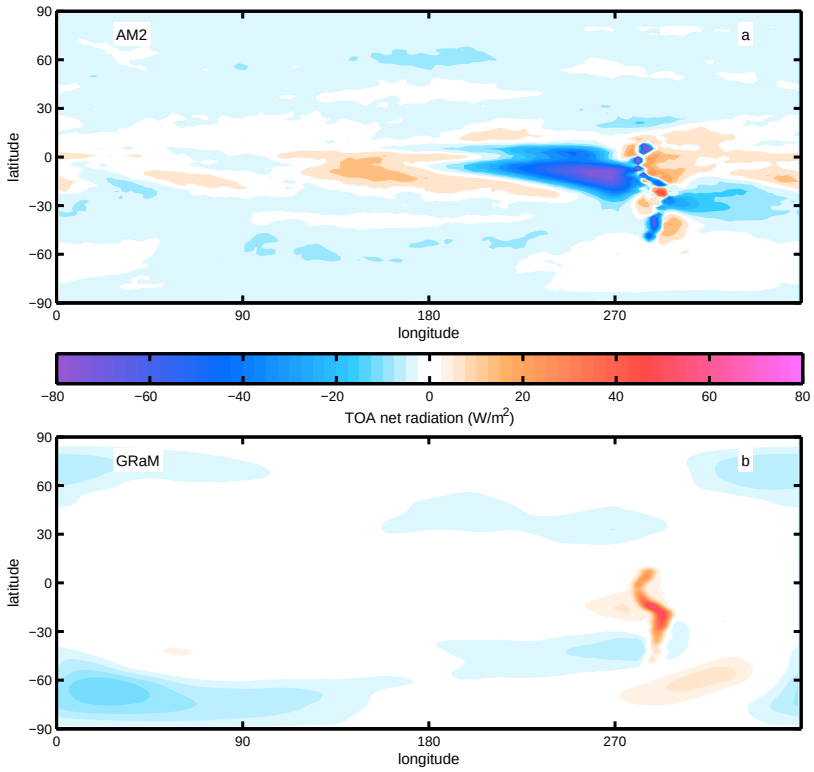

Figure 4.10: RTminusA changes in net total (SW+LW) TOA radiation in AM2 (panel a) and GRaM (panel b). Positive values indicate downward radiation and a gain of energy into the atmosphere.

north and south poles are $\pi/2$ and $-\pi/2$, respectively. Here, SW and OLR fluxes are evaluated at model TOA and are integrated over the respective hemispheres.

The change in total meridional energy transport across the equator is exactly balanced by the change in the net energy that enters the climate system (atmosphere and ocean) in either hemisphere. Comparing simulations that hold $OET^{\phi=eq}$ constant is equivalent to saying that changes in the TOA budget are completely due to changes in energy transport within the atmosphere. To examine where the important regions to changes in the energy transport are, a bit of rearrangement of Equation 4.4 reveals:

$$\int_0^{90} 2\pi a^2 \cos(\phi)(\Delta SW - \Delta OLR)d\phi - \int_0^{-90} 2\phi a^2 \cos(\phi)(\Delta SW - \Delta OLR)d\phi = -2\Delta TET^{\phi=eq} \tag{4.6}$$

In Equation 4.6, since the poleward limit of the integrals is the poles, then Equation 4.6 gives the change in the cross equatorial energy transport do the the hemispheric averaged TOA energy imbalance. Looking at the area of the NH-SH change in the TOA budget shows us the latitudinal contributions to the change in the hemispheric imbalance of absorbed radiation (Figure 4.12). The imbalance in radiation between the hemispheres is related to the cross-equatorial energy transport. In Equation 4.6, note that the NH-SH radiation imbalance is the difference between the radiation in the hemispheres, not the addition of the net radiation in the two hemispheres: if this other quantity were used, then the total area of the curves would be zero since these simulations have reached equilibrium. The schematic in Figure 4.11 translates how a change in the hemispheric imbalance of TOA radiation is related to the cross-equatorial heat transport. Here, a positive change of TOA radiation is defined as an increase in energy absorbed into the atmosphere and a negative change in TOA radiation is a decrease in absorbed energy (an increase in energy emitted by the atmosphere). The hemispheric imbalance is the NH minus SH net (ie, LW+SW) TOA radiation – hereafter call NH-SH Δ TOA, where positive indicates that there is more radiation being absorbed into the NH than into the SH. If the average is posi-

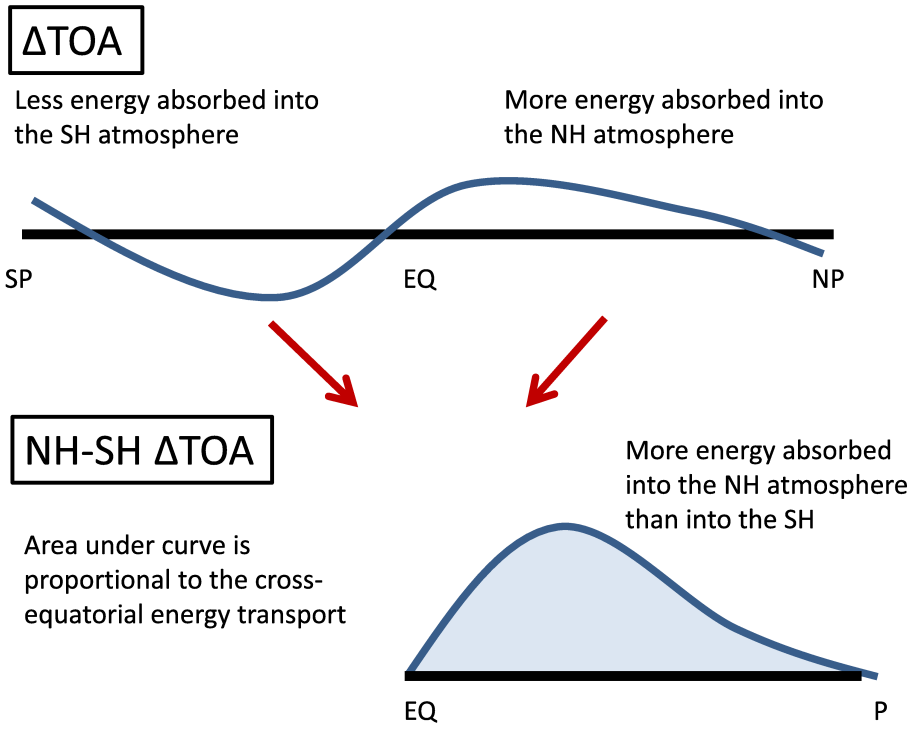

Figure 4.11: Schematic showing how changes in TOA absorbed radiation relates to NH-SH changes in radiation and cross-equatorial energy transport.

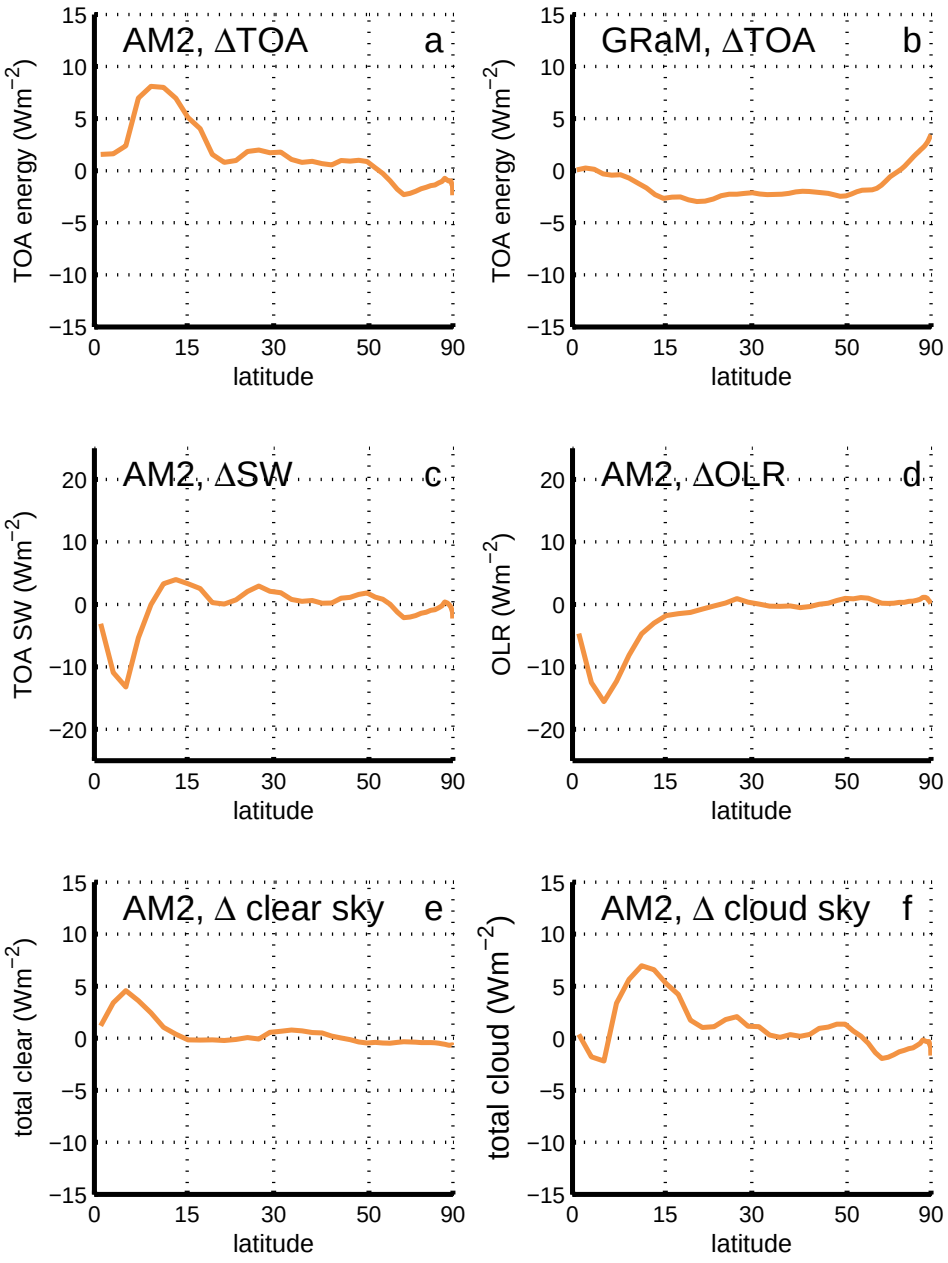

Figure 4.12: RTminusA NH-SH TOA energetic analysis for topography simulations. Panels a (AM2) and b (GRaM) show the differences in the net radiation absorbed in the NH compared to the SH at each latitude for the RTminusA simulation. Panel c shows the NH-SH change in net SW at TOA (positive downward, energy increases in the atmosphere), while panel d shows the NH-SH change in OLR (positive upward, energy leaving the atmosphere). Panel e shows the NH-SH net TOA clear sky radiation, while panel f shows the TOA cloudy sky radiation for AM2 simulations. Positive means that there is a greater change of energy at that latitude in the NH atmosphere, while negative indicates that there is greater energy at that latitude in the SH.

tive, then the change in the NH-SH net TOA imbalance is positive and more energy has been is absorbed in the NH atmosphere than the SH; hence, the change in energy transport across the equator is negative (southward). Conversely, if the average is negative, then there is an increase in energy absorbed in the SH atmosphere than in the NH, and hence, there is an accompanying northward change in energy transport across the equator.

In the AM2 RTminusA difference, the NH-SH area average is positive, indicating that there is greater radiation absorbed in the NH than in the SH because of the addition of topography (Figure 4.12). The change of energy transport across equator in the atmosphere is therefore southward. Anomalously more OLR is emitted in the SH than in the NH, while anomalously more SW is absorbed in the SH than in the NH. However, the change in the hemispheric imbalance of OLR emitted is greater than the change in the hemispheric imbalance in SW absorbed; that is, the change in the imbalance of OLR contributes slightly more to the anomalous southward heat transport. If the change in TOA net radiation is instead split into clear and cloud sky components, then both net cloud and clear sky radiation contribute to the southward change in the cross-equatorial energy transport (Figure 4.12e and f). AM2 total cloud radiation has the greatest positive changes from 5-20°; at these latitudes in the SH, adding a mountain range has increased the low stratus deck, which reduces the absorbed SW insolation. The high clouds in the SH (NH) have also decreased (increased) which allows more (less) OLR. Together, these two effects decrease the energy absorbed in the SH relative to the NH.

As mentioned earlier, the RTminusA change in the net TOA radiation of the GRaM model is different. TOA net SW is constant in GRaM, so the change in TOA radiation is equivalent to the negative of the change in OLR. The change of the hemispheric imbalance in absorbed radiation in GRaM shows that more energy is absorbed in the SH than in the NH (Figure 4.12); there is more OLR anomalously emitted in the NH than in the SH because of the addition of topography, which

indicates a northward change in energy transport across the equator. However, as mentioned before, the reason for this northward transport could be entirely due to numerics in this model when topography is added.

Adding topography to a flat simulation would increase the stationary wave component of the heat transport, and an analysis of the changes in the MMC, stationary eddy, and transient circulation terms of the MSE transport can be done, similar to the analysis of moisture flux convergence in the previous section. However, in calculating the stationary wave component of MSE transport ($[\overline{v^*}\,\overline{MSE^*}]$) the majority of this term is contributed from the mountain range itself. Raising a mountain range increases the zonal anomaly of MSE over the range, which makes the stationary eddy term large in the immediate vicinity of the mountain. Calculating the stationary wave component without including the region in the immediate vicinity of the mountain range would give a better estimate of the change to the stationary wave energy transport elsewhere, despite removing a region that is essential for the energy budget to remain closed. Calculating $[\overline{v^*}\,\overline{MSE^*}]$ without the mountain range shows that the contributions to the stationary eddy transport is small in comparison to changes in energy transport by the MMC.

Adding topography decreases the global mean surface temperature (when compared with the equivalent flat run) in AM2, but not in GRaM (Table 4.2.2, Figure 4.6). This effect occurs even when discounting the small amount of surface that is elevated by the topography. The increase in stratus clouds in AM2 (not present in GRaM) is one possible explanation.

4.3 Changes to the circulation and the momentum budget

The addition of the Andes-like mountains changes the structure of the jets (Figure 4.13). Adding an Andes mountain range in the AM2 model shifts the SH jet poleward and decreases the strength of the NH jet. In GRaM, the jets in both hemispheres are weakened. Atmospheric angular momentum relative to the rotation of the Earth is

	AM2	GRaM
EQ30	286.3	288.0
RT+EQ30	286.6	288.0
EQ10	291.0	288.0
RT+EQ10	290.7	288.0
A	291.1	288.0
NoWES	291.2	288.1
RT+NoWES	291.0	287.9
RT	290.9	288.0
IT	290.6	287.9
RQ	294.1	288.9
RT+RQ	293.6	288.8

Table 4.1: Global mean surface temperature (K) of GRaM and AM2 simulations.

decreased when adding a mountain range. Mountain torque from adding an Andes-like range decreases the atmospheric angular momentum in both models.

In the tropics, if eddies and vertical advection are neglected, then the zonally-averaged momentum budget of the atmosphere reduces to $(f + \overline{\zeta})\overline{v} = 0$. Ignoring eddies is an invalid approximation and using this momentum budget measures how much effect eddies have in the tropics. As the meridional velocity is non-zero, then vorticity and the Coriolis parameter must balance. If $-\overline{\zeta}/f = 1$, then the angular momentum balance is achieved through the zonal and time mean winds. The farther from 1 that $-\overline{\zeta}/f$ is, the more a role that eddies play in driving the Hadley circulation. Eddies remove more momentum from the mean flow in GRaM simulations than in AM2 simulations; this also explains the stronger subtropical jets of AM2 (Figure 3.1). Adding mountains decreases $-\overline{\zeta}/f$ in both models as seen in Figure 4.13. $-\overline{\zeta}/f$ is taken at 220HPa in AM2 and at 340HPa in GRaM because the jets are lower in GRaM. Caculating $-\overline{\zeta}/f$ at a higher level in GRaM gives lower values. In summary, adding mountains increases the role that eddies have in driving the tropical circulation.

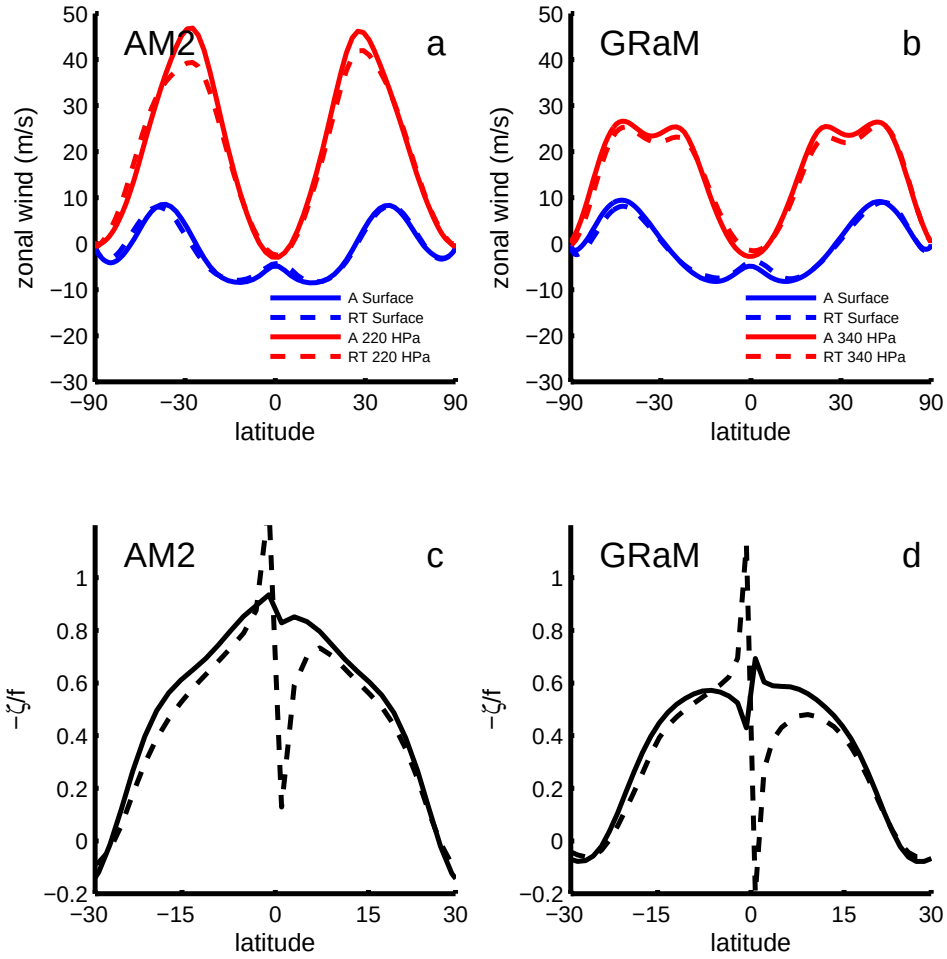

Figure 4.13: RTminusA surface and 220HPa zonal winds in AM2 (panel a) and surface and 340HPa zonal winds GRaM (panel b). Panels c and d show the A (solid line) and RT (dashed line) simulation $\overline{\zeta}/f$ at 220HPa in AM2 (c) and at 340HPa in GRaM (d).

Chapter 5

REMOVAL OF WIND-EVAPORATION FEEDBACK

A hemispheric asymmetry conditions one hemisphere to have greater tropical precipitation than the other. In the previous section, this asymmetry is a SH mountain range and some mechanism to propagate this signal into the NH. Often the WES mechanism is cited. Here, we test if the WES mechanism is present in these model simulations by artificially excluding the wind dependence of evaporation: in calculating evaporation from Equation **??**, $|U|$ is replaced with the symmetrized profile output $|\bar{U}|$ taken from the flat, aquaplanet simulations (marked by the description noWES from here forward). In all other equations, wind in the model evolves naturally. Only in the evaporation parameterization does wind not change with time. There are two simulations presented here for each model that have the wind evaporation feedback, one that is flat (noWES) and one with real-world Andes topography (RT+noWES). Note that the wind dependence of the sensible heat flux has not been altered; since the Bowen ratio in the deep tropics is small, any changes in evaporation would dominate over those in sensible heat anyway.

5.1 The response of removing wind-evaporation feedback in a flat aquaplanet

Removing the WES mechanism in an aquaplanet simulation does not change the mean climatology in a large way (noWESminusA). If WES is important for maintaining convergence in the NH, turning off this parameterization should decrease the asymmetry of precipitation about the equator. Comparing the flat simulations with and without WES (A and noWES simulations, respectively), there is little change in

the zonal-mean wind strength felt by evaporation in each model (Figure 5.1). The wind difference between the simulations with topography and WES (orange) shows that the wind felt by evaporation would otherwise vary much more than it is prescribed. When comparing how evaporation changes in simulations with topography and with/without WES, we see that adding topography results in a similar change in evaporation from the flat simulation with WES regardless of whether WES is present or not. The response of evaporation to topography in these simulations is different in the models, with a southward shift in AM2 and a general tropical decrease in GRaM. The changes in evaporation are almost an order of magnitude smaller than the scale of tropical precipitation changes. The precipitation response is very similar regardless of whether evaporation uses the prescribed or actual surface wind.

The response of precipitation in a flat aquaplanet to turning off a WES feedback in these simulations is small, but shows different results in each model (Figure 5.1). AM2 shows a small southward shift of precipitation when turning off WES, while GRaM shows an intensification of precipitation at the equator. [The aquaplanet simulation with WES in AM2 contained a tiny amount of random asymmetry: symmetrizing the wind strength in the evaporation parameterization likely helped to symmetrize the climate state.] The ITCZ in the aquaplanet AM2 simulation peaked slightly in the NH tropics (see Figure 4.1). Symmetrizing the wind field in evaporation shifted the upward branch of the Hadley cells southward (Figure 5.2). Removing WES in GRaM resulted in stronger Hadley cells which resulted in greater moisture transport to the ITCZ. The greater increase in SH Hadley strength results in more moisture advection in the SH, which is reflected in a greater decrease of precipitation south of the equator than north of it.

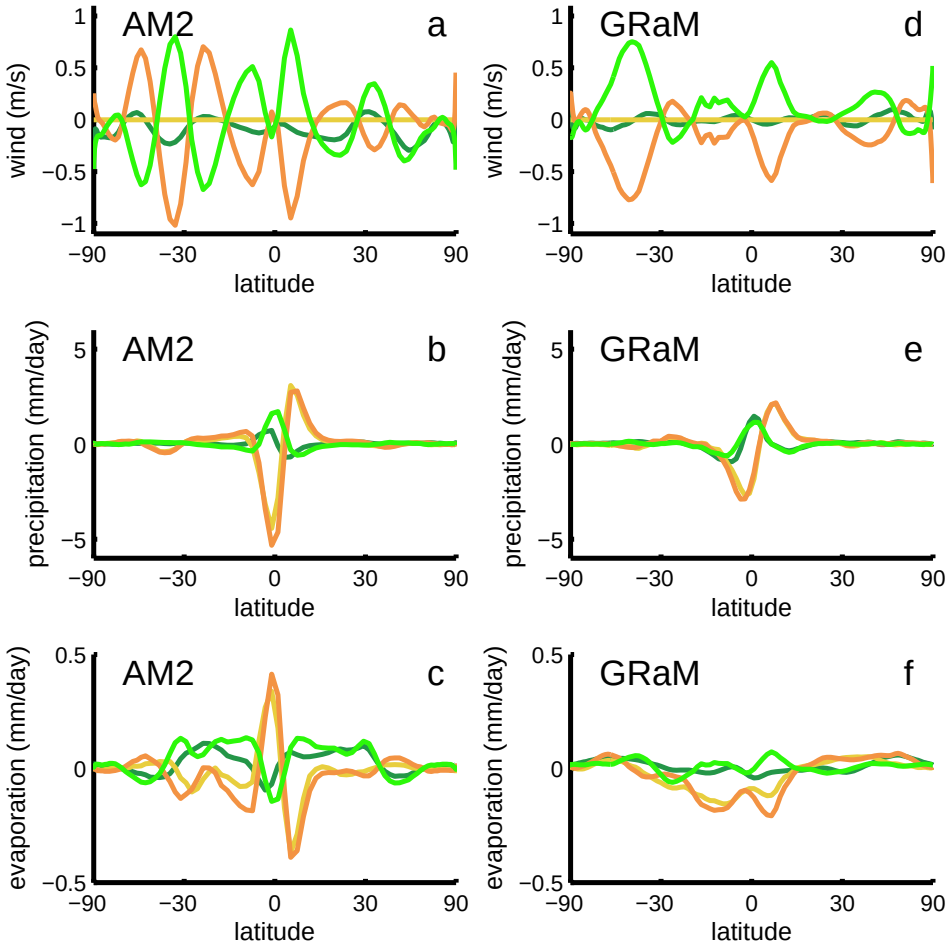

Figure 5.1: Zonal mean changes in precipitation, evaporation, and wind in experiments with and without wind-evaporation feedback. Panels a-c show changes in the AM2 simulations and panels d-f show the changes in the GRaM simulations. The changes in the wind felt by the evaporation parameterization are in panels a and d. Changes in precipitation are in panels b and e, and changes in evaporation are in panels c and f. Differences of NoWESminusWES (dark green), NoWES+RTminusRT (light green), NoWES+RTminusRT (yellow), and RTminusA (orange) are shown.

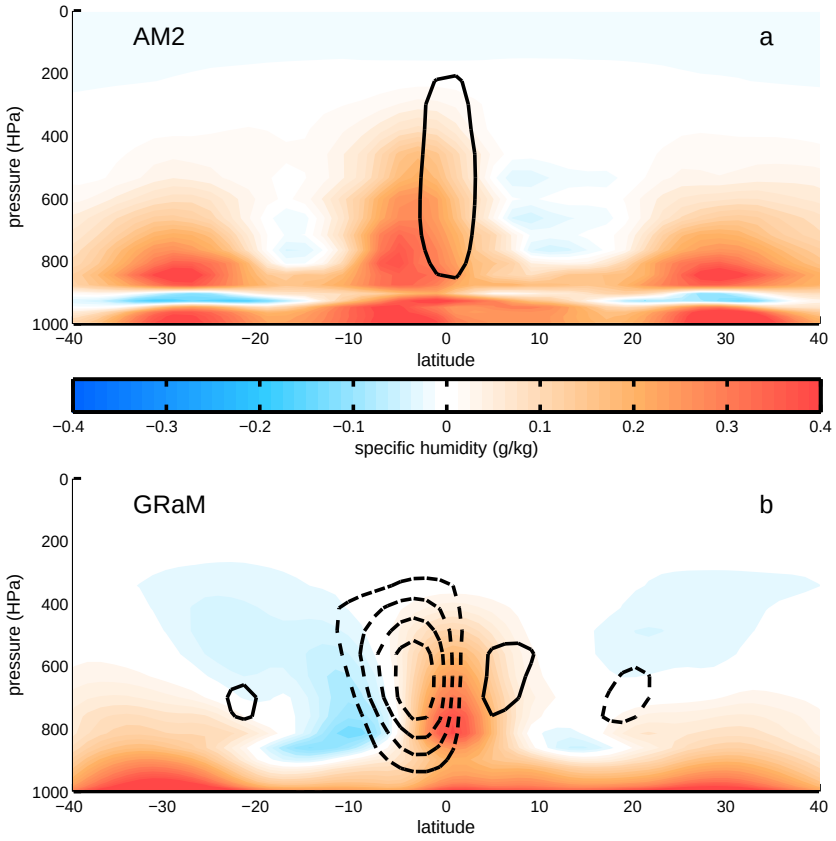

Figure 5.2: NoWESminusWES changes in specific humidity (shading) and streamfunction (contours) in AM2 (panel a) and GRaM (panel b). Contours are spaced every 5×10^9 kg s^{-1}. Solid contours indicate clockwise motion, while dashed contours indicate counterclockwise motion. For comparison, the maximum streamfunction in the Hadley cells of these simulations is 2×10^{11} kg s^{-1}.

5.2 Removal of wind-evaporation feedback in simulations with a SH mountain range

Adding topography shifts the ITCZ northward in both models, even without the wind-evaporation feedback. The difference in the RT+noWESminusnoWES precipitation change and the RTminusA precipitation change is shown in Figure 5.3. This quantity is the difference of adding mountains in a noWES framework versus a WES-included framework. If WES is important the difference will be large; if turning off the wind-evaporation feedback is completely unimportant then the difference will be near zero. Figure 5.3 shows that this difference is small in comparison to the RTminusA precipitation change (Compare Figure 5.3 with Figure 4.1). Both models have a little more precipitation at the equator in the NoWES topography runs, but this is smaller than the amount that the centroid of precipitation shifts.

The change in pattern in evaporation, SST, and stratus clouds (Figure 5.4) between these experiments is also not as large as the differences seen in the RTminusA or RT+noWESminusNoWES changes. The RT+noWESminusNoWES SST change is slightly greater than the RTminusA SST change, but these changes are not as large as the cooling in the subtropics due to the mountains of either model. Hence, with or without WES feedbacks allowed, mountains in GRaM and AM2 shift the ITCZ north.

The impact of mountains is to shift the ITCZ into the NH, with or without WES feedback operating. This suggests that the zonal extent of the precipitation response forced by the mountains is different in the two models because of the differences in stratus cloud feedbacks and not because of differences in WES feedbacks.

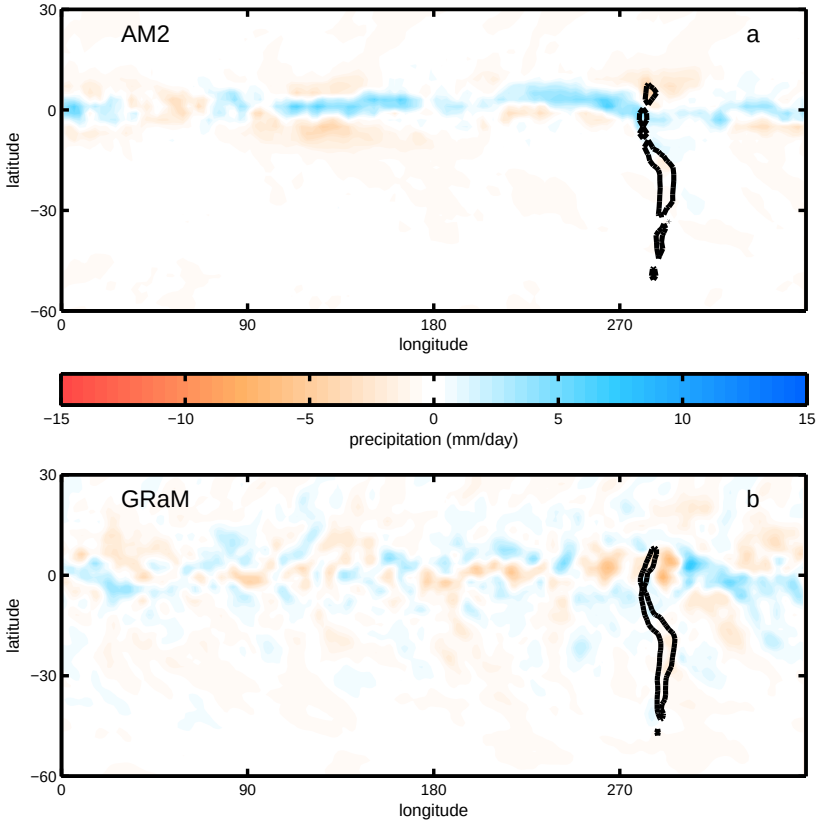

Figure 5.3: The impact of WES in setting the response to realistic topography. The difference of the RT+noWESminusnoWES and RTminusA precipitation changes is shown for AM2 (top panel) and GRaM (bottom panel). Black contours indicates topography higher than 1000m. GRaM fields are Gaussian filtered (bandwidth of 5×10^{-4}).

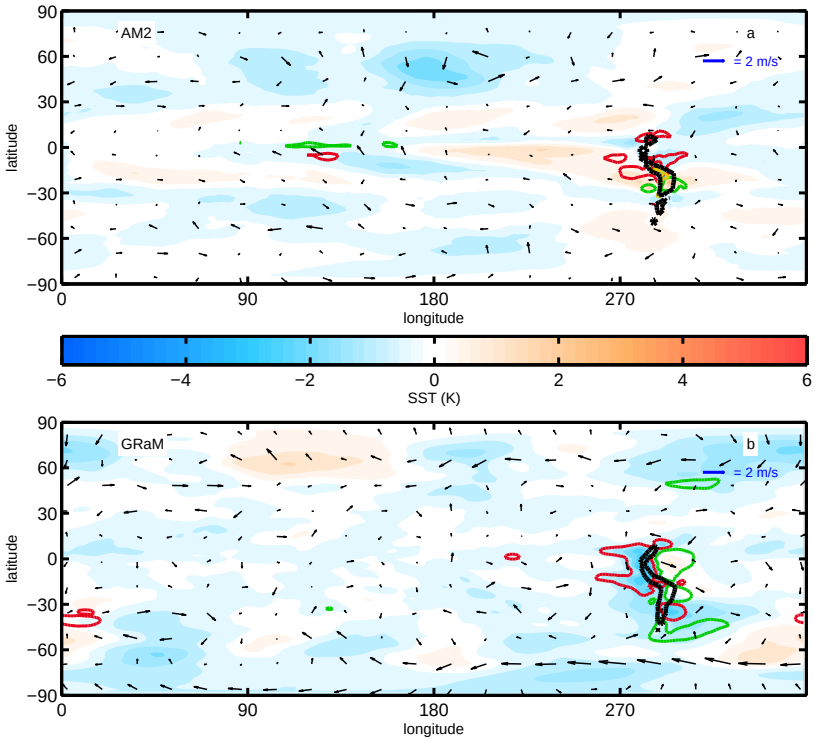

Figure 5.4: The difference between RT+NoWESminusNoWES and RTminusA of SST (shading), evaporation (contours) and wind (vectors) in AM2 (panel a) and GRaM (panel b). Red (green) contours indicate a 10 W m^{-2} increase (decrease) of evaporation in AM2 and 5 W m^{-2} increase (decrease) of evaporation in GRaM. Vectors are the bottom sigma layer winds. Black contours indicates topography higher than 1000m. GRaM fields are Gaussian filtered (bandwidth of 5×10^{-4} m^{-2}).

Chapter 6

THE CLIMATE RESPONSE TO THE ADDITION OF BOTH TOPOGRAPHY AND SURFACE HEAT FLUXES

In the experiments described in the previous sections, there was no prescribed q-flux. In this chapter, we evaluate the sensitivity of the response to the mountains by modifying a q-flux to be (a) the zonal average of the real-world q-flux (RQ) and (b) an idealized midlatitude q-flux (IQ10 and IQ30) used in Kang et al. (2008) and Kang et al. (2009).

6.1 Zonal precipitation response in all simulations

The zonally-averaged precipitation for all simulations is presented in Figure 6.1. Colors are ordered by the expected ITCZ location given previous theories of extratropical q-flux forcing (Kang et al., 2009) and mountain forcing (Takahashi and Battisti, 2007). ITCZ location is computed by interpolating the precipitation field with a cubic spline algorithm and finding the maximum.

The variation of the ITCZ location over all q-flux and topography simulations is larger in the AM2 model than in GRaM: GRaM's profile of precipitation varies little, while AM2's varies wildly, swinging from 16°S to 9°N depending on the q-flux. Cloud and water vapor feedbacks are responsible for the greater range of latitudinal displacement in the experiments using AM2 than those in GRaM. AM2's response is larger than that seen in the real world, as evidenced by the ITCZ location of 8°N in the RQ simulation. Some of this bias is due to the lack of continents and lack of seasonal cycle, which would modulate the response. Radiative feedbacks are the major player for accentuating the impact of both topography and asymmetric heating

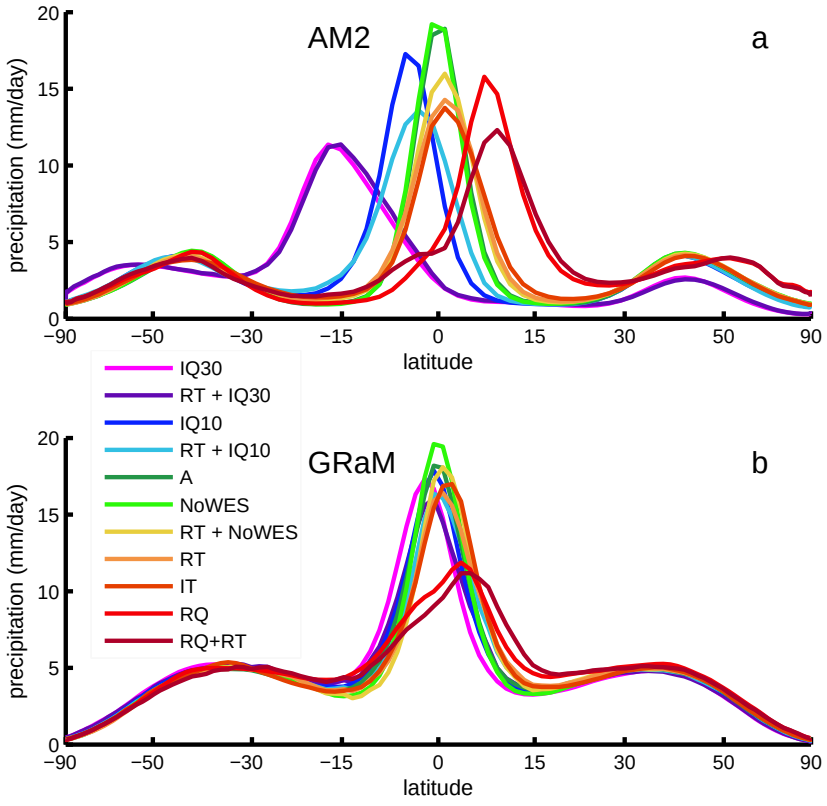

Figure 6.1: Zonally averaged precipitation in all AM2 (panel a) and GRaM (panel b) simulations. Note that the x-axis is area-weighted.

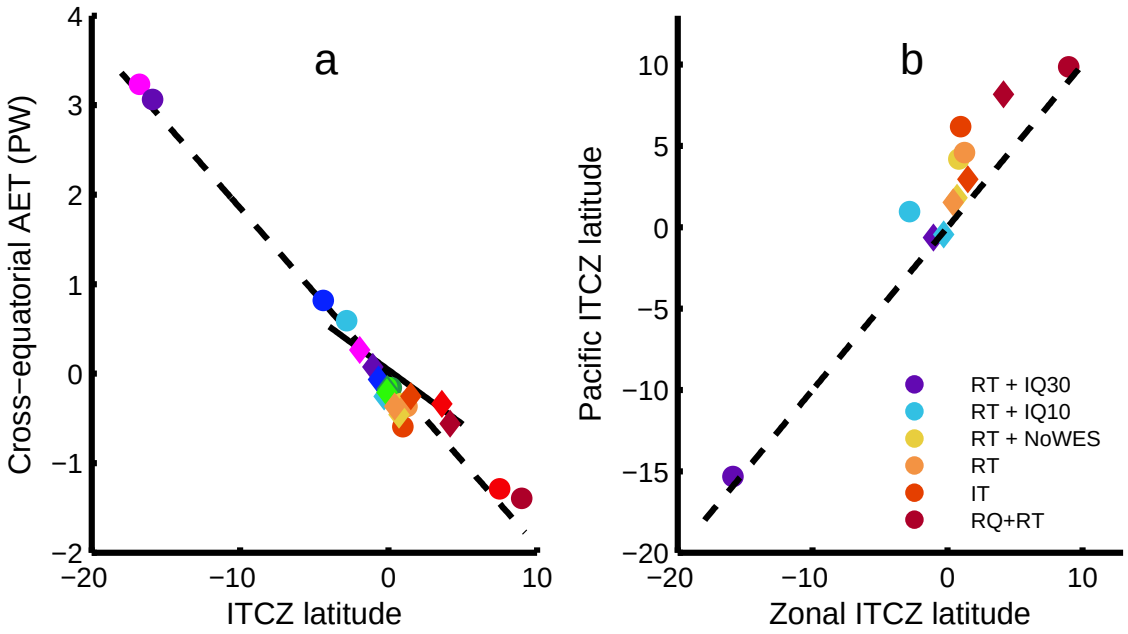

Figure 6.2: ITCZ latitude versus cross-equatorial atmospheric energy transport (panel a) and Global ITCZ location versus Pacific ITCZ location (panel b). Circles correspond to AM2 simulations and diamonds to GRaM. Colors refer to the same simulations as in the legend of Figure 6.1; in panel b, the colors that refer to the simulations with topography are shown. The ITCZ versus $AET^{\phi=eq}$ locations of AM2 and GRaM simulations are linearly regressed to best fit lines that have slopes of -0.19 PW/degree and -0.08 PW/degree and R2 values of 0.98 and 0.46, respectively. In panel b, a one-to-one line indicates if the Pacific ITCZ and the global ITCZ are identical; flat simulations are not included in panel b.

on tropical precipitation.

Mountains are expected to affect the precipitation less since they have a limited regional response, and the results in Figure 6.1 confirm this expectation. In general, q-fluxes used in this study induce a zonal mean response of precipitation that is larger than the mountains response. A "Pacific" ITCZ location is calculated using the zonal average within 120° (50°) longitude to the west of the mountain range in AM2 (GRaM) (Figure 6.2). In the region to the west of the mountain range (where the Pacific ocean would be), the ITCZ is farther north than the global mean ITCZ

location of the same simulation.

The energetic constraint described in Kang et al. (2009) is valid in these simulations, even when adding a mountain range. In both models, the centroid of tropical precipitation varies with the magnitude of the energy transport across the equator (done by the Hadley circulation) (Figure 6.2). With a hemispheric imbalance in radiation absorbed, the Hadley circulation moves energy to the hemisphere with less energy, and the lower branch of the Hadley circulation responds in turn, moving moisture in the opposite direction. Although the range of the ITCZ location is much smaller in GRaM simulations, the energy moved by the circulations in this model is more effective at changing this location: per PW of energy moved across the equator moved by the atmosphere, the ITCZ moves about 12 degrees. In contrast, the ITCZ in AM2 moves approximately 5 degrees per PW of cross-equatorial heat transport. The correlation between ITCZ location and cross-equatorial energy transport is greater in AM2 ($R^2 = 0.98$). The relative effects of topography and asymmetric heating are more similar in GRaM than in AM2. As a result, the goodness-of-fit of the relation between cross-equatorial heat transport and the ITCZ location is not as strong in GRaM.

6.2 An energetic analysis of the addition of q-fluxes in simulations with the same topography

When given an asymmetric surface heating, the atmosphere in AM2 overcompensates while that of GRaM undercompensates (Figure 6.3). Here we define atmospheric compensation as

$$|(AET_X^{\phi=eq} - AET_A^e q)/(OET_X^{\phi=eq} - OET_A^{\phi=eq})| = |\Delta AET^{\phi=eq}/\Delta OET^{\phi=eq}| \quad (6.1)$$

where X denotes an experiment and A denote the aquaplanet experiment with no added ocean heat transport and no mountains. The ratio in Equation 6.1 is the slope in Figure 6.3; overcompensation is indicated by a slope that is steeper than

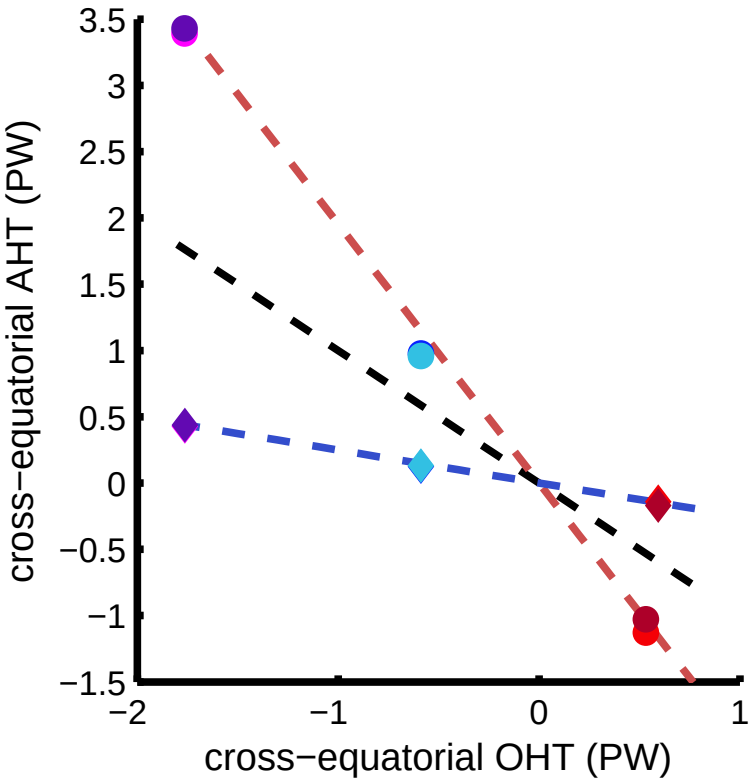

Figure 6.3: Compensation of atmospheric energy transport to the implied ocean energy transport. The black line shows where the simulations of a perfectly compensating model would lie. The red line with steeper slope indicates the overcompensation of AM2 while the blue line with shallower slope indicates the undercompensation of GRaM. Colors refer to the same simulations as in the legend of Figure 6.1. Diamonds are GRaM simulations, while circles are AM2. The symbols for the RT+IQ30 and IQ30 cases are on top of each other, as are the RT+IQ10/IQ10 and the RT+RQ/RQ cases.

the one-to-one line (black line), while a shallower slope indicates that the atmosphere undercompensates. Using a tropical compensation from 20°S-20°N as in Kang et al. (2009), instead of one at the equator does not change this result much, though with this definition, AM2's overcompensation is not quite as large.

Expanding upon this definition of compensation illuminates how the feedbacks in AM2 allow so much overcompensation. As seen in Equation 4.4, total energy transport at the equator must equal the sum of the atmospheric and oceanic energy transports at the equator. If our models atmosphere were to perfectly compensate the applied q-flux, then $\Delta OET^{\phi=eq} = -\Delta AET^{\phi=eq}$ and $\Delta TET^{\phi=eq} = 0$. If the atmosphere overreacts (as in AM2), then $\Delta OET^{\phi=eq} < -\Delta AET^{\phi=eq}$ and $\Delta TET^{\phi=eq} < 0$. The converse holds for an undercompensating atmosphere like GRaM, so that $\Delta TET^{\phi=eq} > 0$.

Figure 6.4 shows scaled TOA net radiative terms while Figure 6.5 shows the hemispheric imbalance of TOA radiation (which are also the integrands of Equation 4.6) for all GRaM (a) and AM2 (b) simulations that include a q-flux. The lines in Figures 6.4 and 6.5 have been scaled by the cross-equatorial OET so that the different q-fluxes are compared equally; this scaling also changes the sign of simulations so that they all correspond to a 1 PW energy transport across the equator that heats the atmosphere in the NH and cools in the SH. The dashed curves show a scaled $\Delta OET^{\phi=eq}$. If the local atmosphere did not respond at all to the q-flux (a local radiative response), then the TOA energetic differences should line up exactly on these dashed lines. If atmospheric transports everywhere exactly respond to the ocean energy transport locally, then the change in the TOA energetic terms should be zero everywhere (a purely dynamic response).

The hemispheric average of the values in Figure 6.5 is equal to $-2\Delta TET^{\phi=eq}$. If the average is negative, then the atmosphere is undercompensating; if positive, the atmosphere is overcompensating. It is notable that the TOA radiation imbalance of both models show the same story in the extratropics: somewhere between a pure radiative and a pure dynamic response. The atmosphere responds locally to the

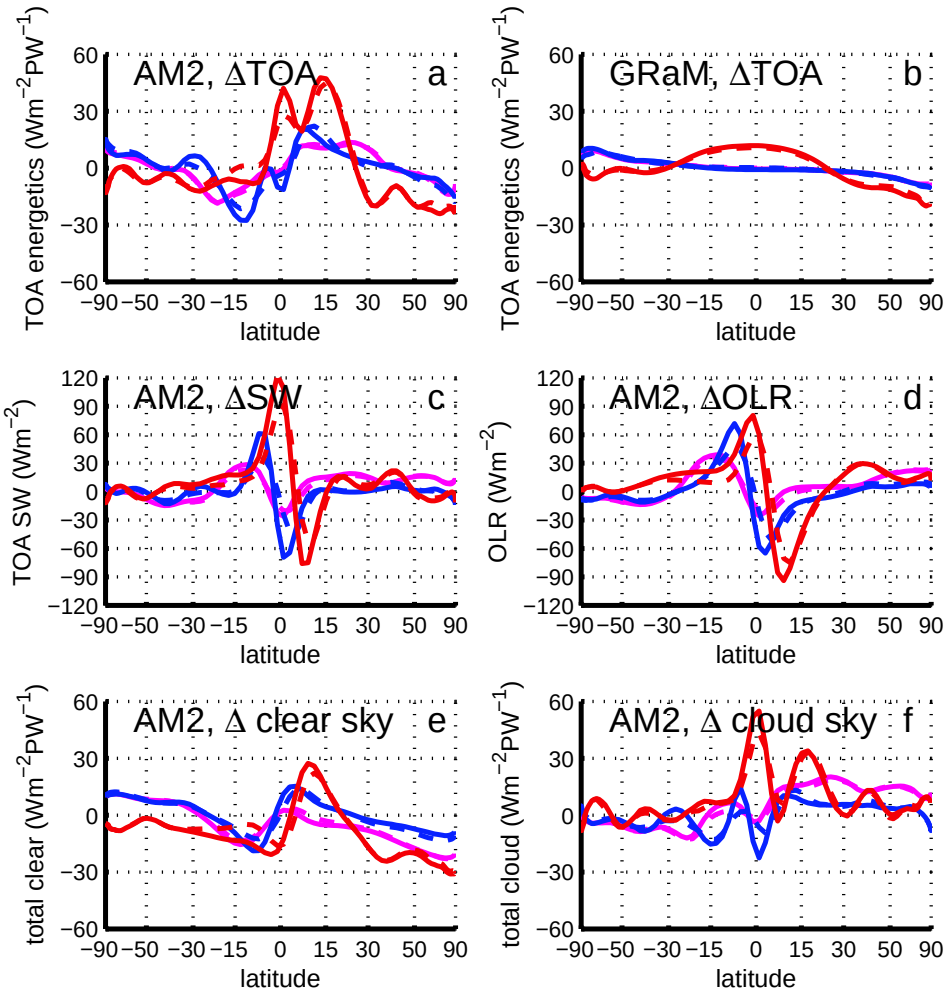

Figure 6.4: Scaled TOA energetics for all q-flux experiments. All values have been scaled by the mean 20°S-20°N ocean energy transport of the simulation. Panels a (AM2) and b (GRaM) show the total (LW+SW) net TOA energy for all surface simulations. Colors refer to the same q-flux experiments as shown in Figure 6.3. Panel c shows the change in SW TOA (positive indicates into the atmosphere), while panel d shows the change in OLR (positive indicating out of the atmosphere). Panel e shows the total net TOA clear sky radiation for AM2 simulations, while panel f shows the total net TOA cloudy sky radiation.

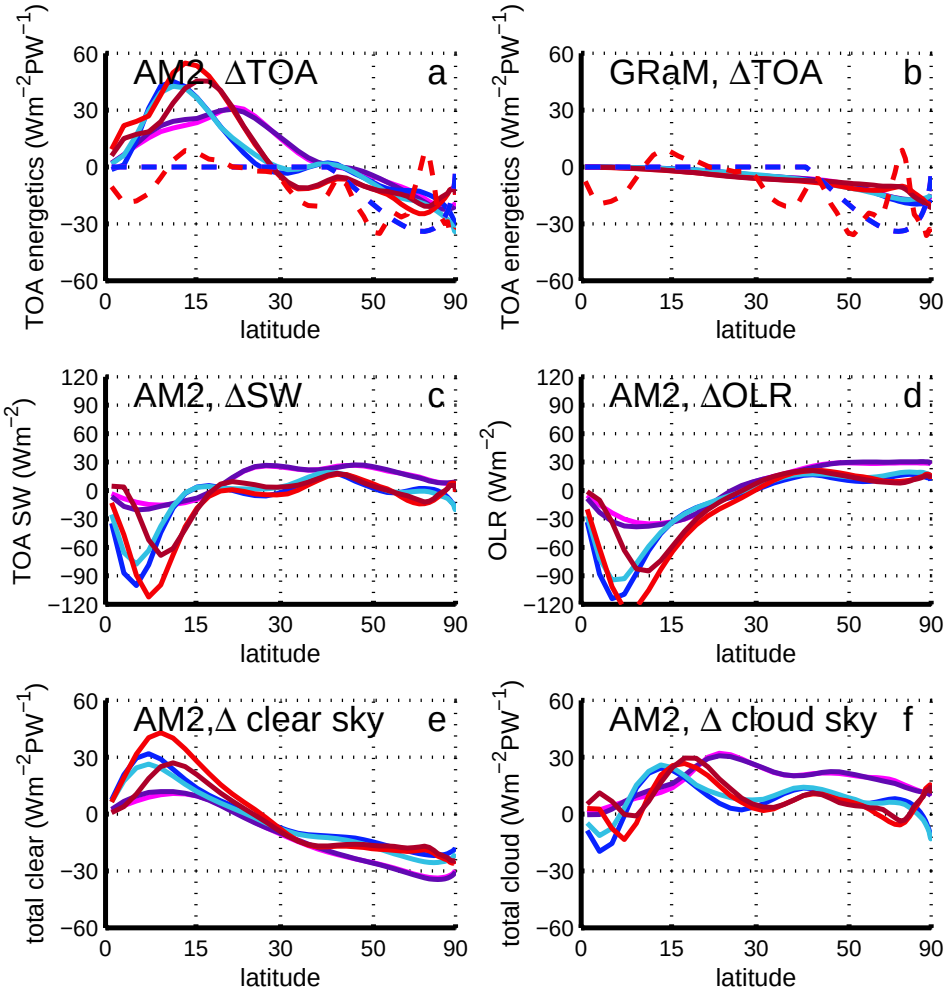

Figure 6.5: Scaled NH-SH TOA energetics, as in Figure 4.12, but for q-flux experiments. All values have been scaled by the mean 20°S-20°N ocean transport of the simulation. Panels a (AM2) and b (GRaM) show the total (LW+SW) net NH minus SH TOA energy for all simulations with q-fluxes. Colors refer to the same q-flux experiments as shown in Figure 6.3. The dashed lines in these two panels indicate the scaled q-flux forcing. If the atmosphere responded completely locally to the forcing, then the TOA energetic term would lie exactly over the dashed line. Panel c shows the NH-SH change in SW TOA (positive indicates into the atmosphere), while panel d shows the NH-SH change in OLR (positive indicating out of the atmosphere). Panel e shows the NH-SH total net TOA clear sky radiation for AM2 simulations, while panel f shows the total net TOA cloudy sky radiation. This figure is the NH-SH equivalent of Figure 6.4.

surface heating by transporting some heat away and by increasing (decreasing) its OLR in the NH (SH). In GRaM, this is the entire story; this heating in the extratropics bleeds gradually into the tropics, and it is the difference of heating in the extratropics that is most important for explaining the cross-equatorial heat transport. The average TOA radiation imbalance is negative. GRaM is under-responding to all the applied q-fluxes nearly linearly, as all the scaled NH-SH TOA radiation terms are approximately collinear.

In AM2, water vapor and cloud feedbacks completely change the response in the tropics, and are largely responsible for the overcompensation. Overall, the change in the AM2 TOA energy imbalance is positive. The atmosphere is transporting more amount heat into the SH than the ocean delivered to the NH. The surface heatings are scaled here such that there is heat added (removed) to the NH (SH) from the surface. However, a positive change in the NH-SH net TOA radiative imbalance indicates that the atmosphere has responded to add even more energy into the NH and remove more energy from the SH. More (less) clear sky OLR in the SH (NH) and more (less) LW cloud warming due to changes in the Hadley circulation are part of this energetic response. With an even greater energy imbalance between the hemispheres, the atmosphere works even harder to transport heat across the equator; hence, the ITCZ shifts far into the NH.

Figure 6.5 decomposes the AM2 TOA radiation imbalance into OLR and net TOA SW, as well as total (OLR + net TOA SW) in clear and cloud skies (refer to Figure 4.11 for how to read these figures). Both net clear sky radiation changes (mostly due to changes in LW water vapor absorption) and cloud radiation changes (both LW and SW) play a role in the overcompensation, but in different latitude bands. The response of net clear sky TOA radiation peaks in the deep tropics, while changes in TOA net radiation in cloudy sky peaks farther into the subtropics. In the extratropics, the decrease (increase) in NH (SH) net TOA clear sky radiation from greater (lesser) water vapor is stronger than the increase (decrease) in NH (SH) net

TOA cloud radiation. Figure 6.4 indicates how much of these NH-SH changes comes from the NH and SH.

In AM2, the different effects of clear and cloud sky radiation on the change in TET sometimes act together and sometimes against each other. A q-flux is added that warms the NH and cools the SH extratropics; this heating is eventually felt into the tropics. Deep convection shifts into the northern hemisphere. Changes in circulation increase (decrease) the specific humidity in the NH (SH). Greater moisture increases (reduces) the greenhouse effect in the NH (SH), which results in less (more) OLR emitted to space in the NH (SH) deep tropics. Less (more) cloud sky OLR is emitted to space in the NH (SH) deep tropics because of higher (lower) cloud top heights; changes in stratus decks is minimal in these simulations, (in the added Andes simulations, stratus clouds play role). In the NH (SH) subtropics, decreased (increased) high clouds reduce (enhance) cloud OLR. The warmer atmosphere in the NH subtropics emits more clear sky OLR despite an enhanced greenhouse. Examining all these changes together in a NH-SH context shows that there is more absorbed cloud and clear net radiation acting to increase the anomalous TET across the equator. Once the ITCZ has shifted off equator, the net absorbed radiation from both cloud and clear acts to make the hemisphere of the ITCZ the hemisphere with greater MSE. The other hemisphere has less MSE, and the net effect is that the Hadley cell has changed to reinforce its energy transport across the equator. The more the ITCZ shifts off the equator in these AM2 simulations, the greater the change in energy transport across the equator. GRaM does not have the cloud and clear sky feedbacks that allow the Hadley circulation to energetically reinforce itself off equator.

In Figure 6.5, all simulations have been scaled by the applied q-flux. If the atmosphere responded linearly to the magnitude of the q-flux, then all simulations would show the same response. In the extratropics, all simulations do seem to be reacting similarly, even the red lines (RQ simulations) which have a significantly different meridional q-flux structure. In AM2, the tropical response is not linear. The dark

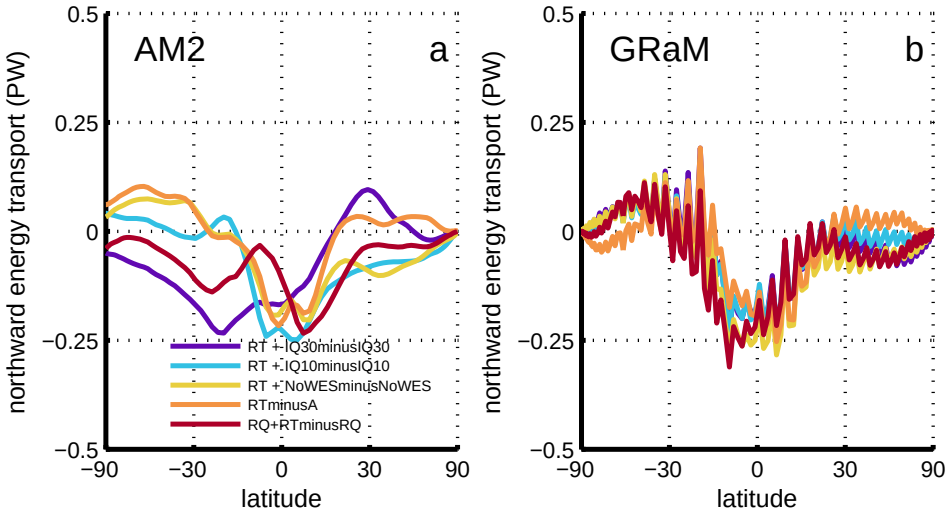

Figure 6.6: Change in energy transport in all simulations that include topography. Panel a and b show the change in total energy transport in AM2 and GRaM simulations that include topography from their equivalent flat simulations. Energy differences shown are IQ30+RTminusIQ30 (purple), IQ10+RTminusIQ10 (blue), NoWES+RTminusNoWES (yellow), RTminusA (orange), RQ+RTminusRQ (dark red).

blue lines indicate simulations with the strongest q-flux (IQ30), and yet, when scaled, the peak of the response is less per PW than simulations with smaller q-fluxes. The width of the ITCZ becomes broader the farther the ITCZ moves from the equator.

6.3 An energetic analysis of the addition of topography in simulations with the same surface heating

Figure 6.6 shows the difference in zonally-averaged atmospheric energy transport of each topography simulation from its flat equivalent. This figure shows the same quantities as in Figure 4.12 a and b, but for all simulations, including those with q-fluxes. If the topography simulation also includes a q-flux, then its climate response is subtracted with the flat simulation that has the same q-flux, leaving only the effect of the added topography. The differences shown in Figure 4.7 are IQ30+RTminusIQ30 (pur-

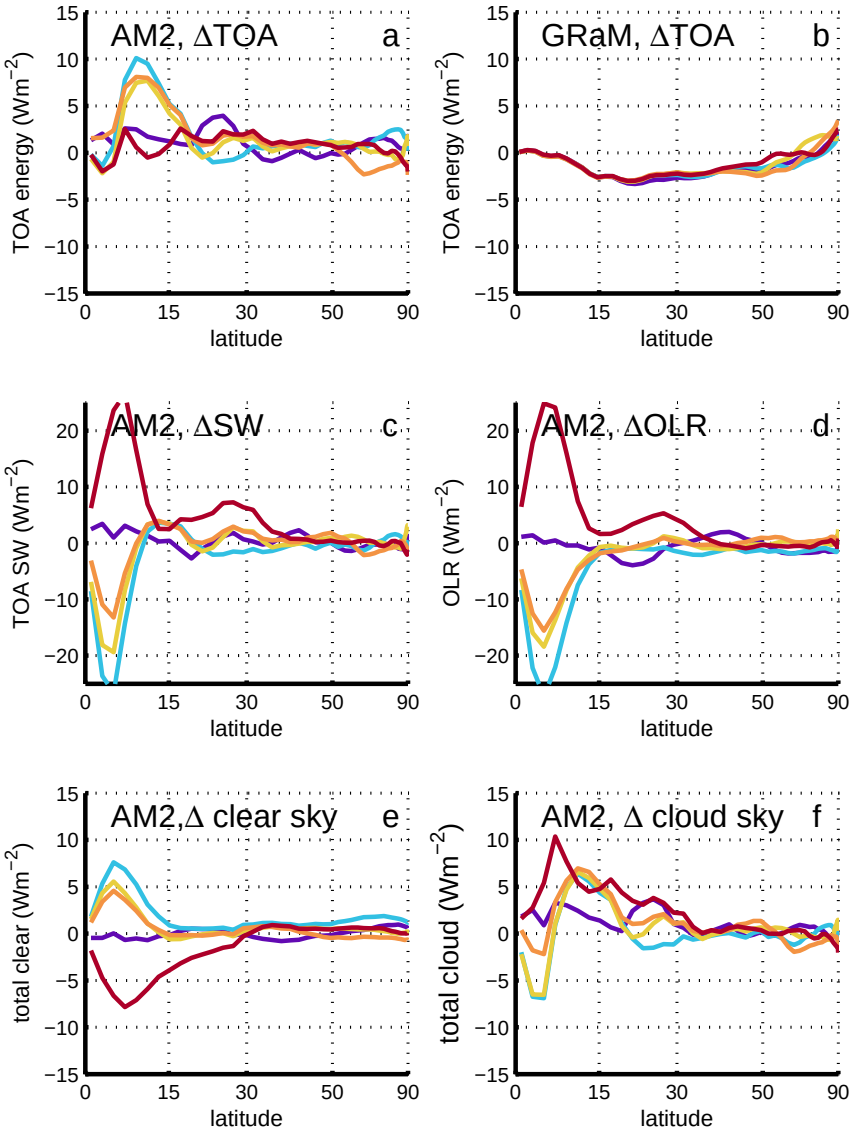

Figure 6.7: NH-SH TOA energetic analysis for topography simulations. Panels a (AM2) and b (GRaM) show the differences in the net radiation absorbed in the NH compared to the SH at each latitude for all simulations that include a SH mountain range. Panel c shows the NH-SH change in net SW at TOA (positive downward, energy increases in the atmosphere), while panel d shows the NH-SH change in OLR (positive upward, energy leaving the atmosphere). Panel e shows the NH-SH net TOA clear sky radiation, while panel f shows the TOA cloudy sky radiation for AM2 simulations. Simulations shown are IQ30+RTminusIQ30 (purple), IQ10+RTminusIQ10 (blue), NoWES+RTminusNoWES (yellow), RTminusA (orange), RQ+RTminusRQ (dark red). Positive means that there is a greater change of energy at that latitude in the NH atmosphere, while negative indicates that there is greater energy at that latitude in the SH.

ple), IQ10+RTminusIQ10 (blue), NoWES+RTminusNoWES (yellow), RTminusA (orange), RQ+RTminusRQ (dark red).

As discussed previously, examining the hemispheric imbalance of TOA radiation indicates which latitudes contribute most to cross-equatorial energy transport. Figure 6.7 shows this difference for the sets of simulations that add topography while holding q-fluxes constant. All GRaM simulations show a similar pattern in TOA imbalance to the addition of topography. The TOA imbalance of AM2 simulations also have a similar pattern but only for those simulations with small q-fluxes that do not shift the upwelling branch of Hadley circulation too far from the equator. The two q-fluxes (IQ30 and RQ) shift the circulation so much that the "equator" of the Hadley circulation is far north or south of the physical equator, and taking differences about the physical equator does not capture these other changes. For the smaller q-flux AM2 experiments, the locations of the radiative response to the addition of topography are similar to the same response in sets of simulations that add a q-flux and hold topography constant (Figure 6.5).

Note that the y-axis of Figure 6.5 has four times the range of those in Figure 4.12, but that zonal average TOA changes in Figure 6.5 are comparable to some of the regional changes in TOA radiation as seen in Figure 4.10. Mountains in AM2 cause a strong local TOA response that is diminished in a zonal mean framework. The radiative response of the atmosphere to an added mountain range is not as strong when seen in a zonal-mean framework. In GRaM, the most noticeable energetic response is a weak decrease in NH SH subtropical TOA energetic terms (where the SH has cooled more). The pattern of tropical clear and cloudy sky changes due to the insertion of mountains in most AM2 simulations is similar to those due to q-fklux forcing albeit weaker in amplitude. With unrealistically large q-flux forcings, the presence of topography has little impact on the position of the ITCZ of the cross-equatorial energy transport. The extratropical response to topography in AM2 is small, while the high latitudes of GRaM have decreased NH-SH OLR, implying that

the SH warms slightly.

Chapter 7

SUMMARY AND CONCLUSIONS

This study has examined how to move the tropical precipitation in two different aquaplaent models. Despite the stark differences in these two aquaplanet models, the results are remarkably similar. Adding a mountain range results in a northward shift in tropical precipitation. The westward extent of the shift is greater in the AM2 simulations. Changes in evaporation are small in both models, which indicates that changes due to the surface wind are also small. Changes in the precipitation are related most to changes in the moisture flux convergence, which in turn is related to changes in the Hadley circulation.

The result that tropical precipitation shifts northward is a robust result in both models with or without wind-evaporation feedback included in the evaporation parameterization. That wind-evaporation feedback is not important in these studies questions its importance in determining the ITCZ location in both basins, though more work needs to be done to show its importance in the Atlantic basin.

Adding extra surface heat into one hemisphere shifts precipitation toward that hemisphere. With a mountain range and q-flux, the effects on the ITCZ are roughly additive. By far, the implied ocean energy transports in these simulations move precipitation farther than an Andes mountain range. Locally, the change of the TOA radiation due to an added Andes range is similar to the analogous TOA changes from a q-flux. In the zonal mean however, adding a q-flux results in a greater shift in tropical precipitation than adding a SH mountain range does.

Including a model without clouds shows the importance of cloud feedbacks on the location of the ITCZ and how feedbacks are important for a model's response.

The stratus cloud deck enhanced in AM2 simulations with an Andes mountain range is important for reflecting insolation, cooling the surface, and making the SH less conducive for deep convection. Changes in the high clouds and moisture due to the shift in the Hadley circulation also play an important role in both simulations that add topography and q-fluxes. In the simulations with q-fluxes, cloud and clear sky feedbacks are responsible for the overcompensation of the AM2 atmosphere to a given q-flux.

These results lend support to recent research showing that the ocean heat flux is important for the location of the ITCZ. Using zonally averaged ocean heat flux derived from observations puts the ITCZ in the correct hemisphere in either model used here. The addition of an Andes range adds for zonal variation in precipitation. The location of the ITCZ is modulated by both local and remote effects, and neither should be neglected when working to understand its dynamics.

Other work on this subject has been undertaken while writing this thesis and will be investigated more fully after this thesis is finished. This other work includes coupled ocean-atmosphere results with slanted ocean basins to test the Philander et al. (1996) slanted coastline thesis. There is also more analysis to be done that looks at the energetic and hydrologic impact of the addition of one continent into an aquaplanet world. Research in this thesis and undertaken while completing this thesis also begs the question of what effect mountains have on the meridional overturning circulation of the ocean. If mountains change the ocean energy transport, then it is possible that the atmosphere energy transport would respond indirectly. Future work after this thesis will be directed either at this question or at other questions of large-scale coupled ocean-atmosphere interactions.

BIBLIOGRAPHY

Adler, R., et al., 2003: The version 2 global precipitation climatology project (gpcp) monthly precipitation analysis (1979-present). *J. Hydrometeor.*, **4**, 1147–1167.

Black, D. E., L. C. Peterson, J. T. Overpack, A. Kaplan, M. N. Evans, and M. K. Kshgarian, 1999: Eight centuries of north atlantic ocean atmosphere variability. *Science*, **286**, 1709–1713.

Broccoli, A. J., K. A. Dahl, and R. J. Stouffer, 2006: Response of the itcz to northern hemisphere cooling. *Geophys. Res. Lett.*, **33**, L01 702.

Chang, P. and S. G. Philander, 1994: A coupled ocean-atmosphere instability of relevance to the seasonal cycle. *J. Atmos. Sci.*, **51**, 3627–3648.

Chiang, J., M. Biasutti, and D. Battisti, 2003: Sensitivity of the atlantic intertropical convergence zone to last glacial maximum boundary conditions. *Paleoceanography*, **18**.

Chiang, J. C. H. and C. M. Bitz, 2005: Influence of high latitude ice cover on the marine intertropical convergence zone. *Clim. Dyn.*, **25**, 477–496.

Dee, D. P., et al., 2011: The era-interim reanalysis: configuration and performance of the data assimilation system. *Quart. J. R. Meteorol. Soc.*, **137**, 553–597.

deMenocal, P., J. Ortiz, T. Guilderson, and M. Sarnthein, 2000: Coherent high- and low-latitude climate variability during the holocene warm period. *Science*, **288**, 2198–2202.

Dima, I. M. and J. M. Wallace, 2003: *J. Atmos. Sci.*, **60**, 1522–1527.

Farneti, R. and G. Vallis, 2009: An intermediate complexity climate model based on the gfdl flexible modelling system. *Geosci. Model Dev*, **2**, 73–88.

Frierson, D. M. W., I. M. Held, and P. Zurita-Gotor, 2006: A gray-radiation aquaplanet moist gcm. part i: Static stability and eddy scale. *J. Atmos. Sci.*, **63**, 2548–2566.

Frierson, D. M. W. and Y.-T. Hwang, 2012: Extratropical influence on itcz shifts in slab ocean simulations of global warming. *J. Climate*, **25**, 720–733.

Fučkar, N. S., S.-P. Xie, R. Farneti, E. A. Maroon, and D. M. W. Frierson, 2013: Influence of the extratropical ocean circulation on the intertropical convergence zone in an idealized coupled general circulation model. *J. Climate*, **26**, 4612–4629.

GFDL, 2004: The new gfdl global atmosphere and land model am2lm2: Evaluation with prescribed sst simulations. *J. Climate*, **17**, 4641–4673.

GFDL, 2006: Gfdl's cm2 global coupled climate models. part i: Formulation and simulation characteristics. *J. Climate*, **19**, 643–674.

Giese, B. and J. Carton, 1994: The seasonal cycle in a coupled ocean-atmosphere model. *J. Climate*, **7**, 1208–1217.

Griffies, S. M., et al., 2005: Formulation of an ocean model for global climate simulations. *Ocean Science*, **1**, 45–79.

Hadley, G., 1735: Concerning the cause of the general trade winds. *Phil Trans, Roy. Soc*, **39**, 58–62.

Haug, G. H., K. A. Hughen, D. M. Sigman, L. C. Peterson, and U. Rohl, 2001: Southward migration of the intertropical convergence zone through the holocene. *Science*, **293**, 1304–1308.

Held, I. M., 2005: The gap between simulation and understanding in climate modeling. *Bull. Amer. Meteor. Soc.*, **86**, 1609–1614.

Held, I. M. and A. Y. Hou, 1980: Nonlinear axially symmetric circulations in a nearly inviscid atmosphere. *J. Atmos. Sci.*, **37**, 515–533.

Hwang, Y.-T. and D. M. W. Frierson, 2013: Link between the double-intertropical convergence zone problem and cloud bias over southern ocean. *Proc. Nat. Acad. Sci.*

Kang, S. M., D. M. W. Frierson, and I. M. Held, 2009: The tropical response to extratropical thermal forcing in an idealized gcm: The importance of radiative feedbacks and convective parameterization. *J. Atmos. Sci.*, **66**, 2812–2827.

Kang, S. M., I. M. Held, D. M. W. Frierson, and M. Zhao, 2008: The response of the itcz to extratropical thermal forcing: Idealized slab-ocean experiments with a gcm. *J. Climate*, **21**, 3521–3532.

Klein, S. A. and D. L. Hartmann, 1993: The seasonal cycle of low stratiform clouds. *J. Climate*, **6**, 1587–1606.

Koutavas, A. and J. Lynch-Stieglitz, 2003: Glacial-interglacial dynamics of the eastern equatorial pacific cold tongue-intertropical convergence zone system reconstructed from oxygen isotope records. *Paleoceanography*, **18**, URL `http://dx.doi.org/10.1029/2003PA000894`.

Lindzen, R. and A. Hou, 1988: Hadley circulations for zonally averaged heating centered off the equator. *J. Atmos. Sci.*, **45**, 2416–2427.

Lindzen, R. and S. Nigam, 1987: On the role of sea surface temperature gradients in forcing low level winds and convergence in the tropics. *J. Atmos. Sci.*, **44**, 2418–2436.

Liou, K. N., 2002: *An Introduction to Atmospheric Radiation*. 2d ed., Academic Press, 51-54 pp.

Liu, Z. and M. Alexander, 2007: Atmospheric bridge, oceanic tunnel, and global climatic teleconnections. *Rev. Geophys.*, **45**.

Mechoso, C. R., et al., 1995: The seasonal cycle over the tropical pacific in coupled oceanatmosphere general circulation models. *Mon. Wea. Rev*, **123**, 2825–2838.

Mitchell, T. P. and J. M. Wallace, 1992: The annual cycle in equatorial convection and sea surface temperature. *J. Climate*, **5**, 1140–1156.

Peixoto, J. P. and A. H. Oort, 1992: *Physics of Climate*. American Institute of Physics, New York.

Peterson, L. C., G. H. Haug, K. A. Hughen, and U. Rhl, 2000: Rapid changes in the hydrologic cycle of the tropical atlantic during the last glacial. *Science*, **290**, 1947–1951.

Philander, S. G. H., D. Gu, G. Lambert, T. Li, D. Halpern, N.-C. Lau, and R. C. Pacanowski, 1996: Why the itcz is mostly north of the equator. *J. Climate*, **9**, 2958–2972.

Schumacher, C. and R. A. Houze, 2003: The trmm precipitation radar's view of shallow, isolated rain. *J. Appl. Meteor.*, **42**, 1519–1524.

Takahashi, K. and D. S. Battisti, 2007: Processes controlling the mean tropical pacific precipitation pattern. part i: The andes and the eastern pacific itcz. *J. Climate*, **20**, 3434–3451.

Thompson, L. G., E. Mosley-Thompson, and K. A. Henderson, 2000: Ice-core palaeoclimate records in tropical south america since the last glacial maximum. *J. Quat. Sci.*, **37**, 377–394.

Tomas, R. A. and P. J. Webster, 1997: The role of inertial instability in determining the location and strength of near-equatorial convection. *Q. J. R. Meteorol. Soc.*, **123**, 1445–1482.

Vallis, G., 2005: *Atmospheric and Oceanic Fluid Dynamics*. Cambridge University Press.

Wielicki, B. A., B. R. Barkstrom, E. F. Harrison, and J. E. C. R. B. Lee, G. L. Smith, 1996: Clouds and the earth's radiant energy system (ceres): an earth observing system experiment. *Bull. Amer. Meteor. Soc.*, **77**, 853–868.

Xie, S.-P., 1996: Westward propagation of latitudinal asymmetry in a coupled oceanatmosphere model. *J. Atmos. Sci.*, **53**, 3236–3250.

Xie, S.-P., 2005: The shape of continents, air-sea interaction and the rising branch of the hadley circulation. *The Hadley Circulation: Present, Past and Future*, H. F. Diaz and R. S. Bradley, Eds., Springer, chap. 5, 121–152.

Xie, S.-P. and S. G. H. Philander, 1994: A coupled ocean-atmosphere model of relevance to the itcz in the eastern pacific. *Tellus*, **46A**, 340–350.

Yoshimori, M. and A. J. Broccoli, 2008: Equilibrium response of an atmospheremixed layer ocean model to different radiative forcing agents: Global and zonal mean response. *J. Climate*, **21**, 4399–4423.

Yoshimori, M. and A. J. Broccoli, 2009: On the link between hadley circulation changes and radiative feedback processes. *Geophys. Res. Lett.*, **36**, L20 703.

Zhang, C., 2001: Double itczs. *J. Geophys. Res.*, **106**, 11 785–11 792.

Zhang, R. and T. L. Delworth, 2005: Simulated tropical response to a substantial weakening of the atlantic thermohaline circulation. *J. Climate*, **18**, 1853–1860.